Production rate calculations for cosmic-ray-muon-produced ^{10}Be and ^{26}Al benchmarked against geological calibration data

Greg Balco[a,*]

[a] *Berkeley Geochronology Center, 2455 Ridge Road, Berkeley CA 94709 USA*

Abstract

First, I benchmark existing methods of calculating subsurface ^{26}Al, ^{10}Be, and ^{14}C production rates due to cosmic-ray muons against published calibration data from bedrock cores and mine excavations. This shows that methods based on downward propagation of the surface muon energy spectrum fit calibration data adequately. Of these methods, one that uses a simpler geographic scaling method based on energy-dependent attenuation of muons in the atmosphere appears to fit calibration data better than a more complicated one that uses the results of a global particle transport model to estimate geographic variation in the surface muon energy spectrum. Second, I show that although highly simplified and computationally much cheaper exponential function approximations for subsurface production rates are not globally adequate for accurate production rate estimates at arbitrary location and depth, they can be used with acceptable accuracy for many exposure-dating and erosion-rate-estimation applications.

Keywords: cosmogenic-nuclide geochemistry, exposure-age dating, erosion rate measurement, production rate calibration, beryllium-10, aluminum-26, carbon-14

1. Introduction

Naturally occurring cosmic-ray-produced nuclides that are useful for geochronology and other Earth science applications, for example ^{26}Al and ^{10}Be, are produced in part by interactions with cosmic-ray muons. At the Earth's surface, production of these nuclides is predominantly due to interaction with high-energy neutrons, and muon interactions account for a small fraction of total production. However, the stopping distance of muons in rock is much longer than that of neutrons, so in the subsurface below a few meters depth, muon interactions account for nearly all cosmogenic-nuclide production. Thus, for geological applications of cosmogenic-nuclide geochemistry in which samples are exposed to the subsurface cosmic-ray flux, it is necessary to accurately estimate production rates due to muon interactions.

*Corresponding author. Tel. 510.644.9200 Fax 510.644.9201
Email address: balcs@bgc.org (Greg Balco)

Preprint submitted to Quaternary Geochronology; this is revision after 2 reviews *January 6, 2017*

Several different methods for computing production rates due to muon interactions are widely used at present. All these methods include calibrated parameters, either formally defined nuclear interaction cross-sections or empirical scaling constants based on simplified physics, that can variously be measured directly by muon irradiation of mineral targets in the laboratory or estimated from geological calibration data. Here 'geological calibration data' means measurements of concentrations of naturally occurring cosmic-ray-produced nuclides in settings where independent knowledge of the geological history of the site allows one to infer nuclide production rates from the concentration measurements.

The purpose of this paper is to benchmark currently available muon production rate calculation methods against the existing set of geological calibration data, as a means of determining (i) how accurate the calculation methods are, and (ii) whether they are accurate enough for common geological and geochronological applications. First, I fit each production rate calculation method to calibration data in order to determine whether or not the method adequately fits the observations, and also to estimate values of interaction cross-sections or other fitted parameters. Second, based on these results, I evaluate the suitability of each method for common applications.

In this paper I consider production by muon interactions of ^{10}Be, ^{26}Al, and ^{14}C in quartz. Although there exist cross-section estimates and geological calibration data that can be used to also estimate cosmic-ray muon production of ^{36}Cl and ^{21}Ne in various target minerals, I do not discuss these nuclides.

2. Muon production rate calculation methods.

Muon production of ^{10}Be, ^{26}Al, and ^{14}C in quartz takes place via two processes: capture of stopped negative muons (henceforth, "negative muon capture") and reactions with high-energy muons (henceforth, "fast muon interactions"). Dunai (2010) provides a comprehensive summary and Heisinger et al. (2002a,b) a detailed description of the production mechanisms; a brief summary follows. As muons originally incident on the Earth's surface travel through rock, they gradually lose energy by a variety of nuclear interaction processes and eventually come to a stop. At this point negative muons may be captured by a target nucleus to produce nuclides of interest. "Fast" muons, that is, muons that have not yet stopped of their own accord due to energy loss, may also produce these nuclides by a variety of higher-energy reactions. Muons incident at the Earth's surface span both a range of incidence angles and a wide spectrum of energies from near zero to very high energies capable of penetrating to depths of thousands of meters. Thus, both negative muon capture and fast muon interactions occur at all depths. Muons with lower energies and/or flatter incidence angles will stop at shallower depths, so as the depth below the surface increases, the remaining muon flux is more energetic and more collimated. For the nuclides of interest here, negative muon capture accounts for the majority of muon production in the upper few meters below the surface. However, the production rate due to negative muon capture decreases more rapidly with depth than fast muon production, so fast muon production is more important at greater depths.

Two classes of methods for calculating muon production rates are in use for Earth science applications at present. The first class is described by Heisinger et al. (2002a,b).

This approach (i) begins with a specified energy spectrum and angular incidence distribution of cosmic-ray muons at the Earth's surface, (ii) computes the stopping rate of muons with particular energy and incidence angle as a function of depth below the surface, and then (iii) integrates over energy and incidence angle to obtain integrated muon fluxes and stopping rates as a function of depth. One can then multiply the stopping rate at a given depth by a likelihood of nuclide production by negative muon capture, and multiply the muon flux at a given depth by a cross-section for nuclide production by interaction with fast muons, to obtain nuclide production rates by these two processes. This method has two important features. First, it accurately represents what is happening physically, specifically that the muon flux becomes more collimated and more energetic with depth. Second, the interaction cross-sections can be determined from laboratory experiments using artificially generated muon beams. Heisinger and others carried out these experiments, and these cross-section measurements are tabulated in the two papers cited above. This method, therefore, allows one to calculate production rates in natural settings entirely from the surface muon spectrum and parameters determined in laboratory experiments, so, in principle, no geological calibration is necessary (however, as discussed later, it appears that geological calibration provides more accurate cross-section estimates for the muon energy range of interest for geological applications). The key disadvantage of this method is that it is computationally somewhat time-consuming because computing the muon fluxes at a particular location and depth requires a numerical integration. For any application that requires integrating production rates during a long exposure history in which a sample's depth varies over time, computation time can be significant.

In this paper I consider two implementations of the Heisinger method. Both use the same method of integration over energy and incidence angle, but they differ in how the muon spectra at the surface are specified.

One implementation, henceforth called "Method 1A," is a MATLAB implementation from Balco et al. (2008) in which the muon energy spectrum at the surface varies with atmospheric pressure exponentially with energy-dependent attenuation lengths taken from Boezio et al. (2000). In this method, the muon energy spectrum does not vary with position in the Earth's magnetic field. Specifically, in Method 1A I use the MATLAB scripts 'P_mu_total.m' and 'P_mu_total_alpha1.m,' version 1.2, dated September 2016 (all computer code used or described in this paper is available online; see Section 12).

The second implementation, henceforth "Method 1B," is a modification of this code by Lifton et al. (2014) in which the muon energy spectrum at the surface varies with atmospheric pressure, geomagnetic cutoff rigidity, and solar modulation according to Sato et al. (2008). Note that solar modulation is relatively unimportant for muon production, and in applying Model 1B throughout this paper I assume that the solar modulation constant is always the mean Holocene value according to Lifton et al. (2014). Specifically, Method 1B uses the MATLAB function 'P_mu_totalLSD.m,' version 1.0, dated March 2011, and an accompanying parameters file dated October 2013, both supplied by Nat Lifton.

Both Methods 1A and 1B use the same method for calculating the subsurface muon fluxes and stopping rates, and thence the nuclide production rates, from a specified surface muon energy spectrum. The difference between them, as described in the preceding paragraphs, lies in how the muon energy spectrum at the surface is specified. Both implementations fully specify the muon flux and stopping rate at any arbitrary location and depth below the surface. To compute nuclide production rates, then, they require measured or calibrated values for (i) a likelihood of production by capture of stopped negative muons, and (ii) a cross-section for production by fast muon interactions, for the nuclide-target mineral pair of interest.

The second class of calculation methods does not compute the muon flux by integration of surface spectra as is done in the Heisinger method. In fact, it does not compute muon fluxes or stopping rates at all. Instead, muon production rates are simply approximated by an exponential function, or a sum of several exponential functions, in mass depth below the Earth's surface. This approach has been used by several authors, for example, by Granger and Smith (2000) and, recently, Braucher et al. (2011) and Braucher et al. (2013). The advantage of this method is that it is computationally trivial, so lends itself to situations in which cosmogenic-nuclide production rates must be integrated over time as a sample changes depth. The disadvantage is that it does not correctly represent the physics of muon production: because the muon flux becomes more collimated and more energetic with increasing depth, the instantaneous e-folding length for muon production continually increases with depth. This effect cannot be represented with a finite sum of exponential functions. Mainly, the importance of this method is that it is computationally extremely simple and also, most likely, accurate enough for many geological applications.

A recent implementation of the exponential-approximation approach (Braucher et al., 2013) computes subsurface production rates due to muons for a particular nuclide-mineral pair by assuming that total muon production as a function of depth at a specific site is exponential in mass depth and defined by a surface production rate and a subsurface e-folding length. They found that apparent subsurface e-folding lengths were similar at various locations where subsurface calibration data existed (with an average of 4380 ± 650 g cm^{-2} for ^{10}Be and ^{26}Al, excluding one outlier), and they assumed that the surface production rate varies exponentially with atmospheric depth with an e-folding length in the atmosphere obtained from previously published atmospheric muon flux measurements. Henceforth I will refer to this approach as 'Method 2.' Method 2 is purely empirical and defines subsurface production rates at arbitrary location and depth for a particular nuclide-mineral pair as a function of two parameters derived from fitting to geological calibration data: a reference surface production rate at 1013.25 hPa atmospheric pressure, and a subsurface e-folding length. Compared to other exponential-approximation methods, this method has two advantages. One, it is very simple. Two, in contrast to most other published applications of the exponential-approximation method, it includes a geographic scaling method.

3. Geoscience applications that require muon production rates to be calculated.

Here I consider three classes of Earth science applications of cosmogenic-nuclide geochemistry that require calculations of production rates due to muons: surface exposure dating; surface erosion rate measurements; and burial dating (with the related application of depth-profile dating). These classes of applications have very different requirements for how precise the muon production rate calculations must be to maintain the desired precision in the eventual quantity being measured, e.g., an age or an erosion rate. Potentially, therefore, some applications could accept reduced precision in calculating production rates due to muons in exchange for computational speed and simplicity, without significantly compromising the overall results.

Exposure-dating applications are for nearly all practical purposes concerned with surfaces that have low erosion rates. Thus, the cosmogenic-nuclide concentration that is measured is the result of production very close to the surface, where production is nearly all by high-energy neutron spallation. At most a few percent of surface production is due to muon interactions (with the exception of in-situ-produced cosmogenic ^{14}C in quartz, where ca. 10% of surface production is due to muons). At present, typical measurement uncertainty on ^{10}Be concentrations in exposure-dating applications, for example, is 3%, and typical uncertainties in estimating total surface production rates are at least 5%, leading to total uncertainties in exposure age near 6% in most cases. Suppose our goal is for uncertainty in muon production rates to contribute only 10% of this total uncertainty. If muon production is 2% of total surface production, we can accept a 30% uncertainty in estimating the surface muon production rate and still achieve this goal. Thus, exposure-dating applications do not require very precise estimates of surface production rates due to muons, and do not require estimates of subsurface production rates at all.

Erosion-rate applications exploit the fact that surface erosion advects subsurface rock or soil through a near-surface layer in which cosmogenic-nuclide production occurs. The faster the erosion rate, the shorter its residence time in the production zone, and the lower the nuclide concentration in a particular package of material when it reaches the surface. Thus, the surface nuclide concentration is inversely proportional to the erosion rate. Relating surface nuclide concentrations to erosion rates requires computing the integrated production during the entire subsurface residence time of the sample, a significant part of which is typically spent below several meters depth where production is entirely by muons. At high erosion rates, up to ~25% of the total surface nuclide concentration can be muon-produced (note that this calculation applies to ^{10}Be and ^{26}Al: this fraction would be larger for *in-situ*-produced ^{14}C, although this nuclide is not generally used for erosion rate estimates). Thus, in relation to the case of surface exposure dating where all relevant production takes place at the surface, maintaining desired precision on an erosion rate estimate requires better precision on estimating muon production. However, we are not concerned with how precise the estimate of the muon production rate is at any particular depth, but rather with how precisely we have computed the integrated muon production over the entire period in which the sample is advected to the surface. Thus, we could potentially accept a method that was inaccurate at any particular depth, but resulted in an accurate computation of the integral production.

Burial-dating applications (Granger, 2006), and also the related category of depth-profile dating applications (see summary in Hidy et al., 2010) are the most demanding application from the perspective of computing production rates due to muons. This is mainly because they involve subsurface samples whose measured nuclide concentration may be nearly entirely muon-produced. In addition, in many of this class of applications, samples have resided at the same depth for long periods of time, so it is necessary to accurately compute the production rate at a specific depth, rather than an integrated production rate over a range of depths. Commonly in this application, the uncertainty in the burial (or depth-profile) age might be dominated by the uncertainty in the estimate of subsurface production rates by muons: in contrast to the situation of surface exposure dating discussed above, a 30% uncertainty in estimating production rates due to muons might contribute a 10-15% uncertainty to a burial age or a 30% uncertainty to a depth-profile age. To summarize, although there exist some variants of burial dating that are less sensitive to this issue (e.g., the isochron method of Balco and Rovey, 2008), these applications are, in general, the most demanding from the perspective of muon production rate calculations in that they require a precise estimate of the muon production rate at a particular depth and location.

4. Geological calibration data.

4.1. What are geological calibration data exactly?

Geological calibration data that can be used to estimate production rates due to muons consist of measured nuclide concentrations in rock that is approximately 1000 g cm^{-2} or more below the surface, such that the measured concentration is entirely due to muon production and not to high-energy neutron spallation. Ideally, one could obtain calibration data from a site where the rock mass had experienced a single period of exposure, of independently known duration, at the beginning of which the nuclide concentration was zero, and during which zero surface erosion took place. So far it has not been feasible to find a site that has all these properties and also where the period of exposure has been long enough that nuclide concentrations below several meters depth would be accurately measurable. Instead, therefore, existing calibration data come from drill cores and mine excavations at sites where (i) the surface erosion rate is relatively low, and (ii) geologic evidence indicates that the surface has been steadily eroding at this low rate for an extended time, ideally millions of years, such that nuclide concentrations have reached a steady state in which nuclide production at a certain depth is balanced by loss by radioactive decay and advection of material towards the surface due to erosion.

In this case, the workflow goes as follows. First, measure the surface nuclide concentration, which is nearly all due to spallogenic production, and apply an independently calibrated spallogenic production rate estimate to determine the erosion rate. Second, measure the nuclide concentration in the subsurface where spallogenic production is zero. The nuclide concentration is related to the production rate as follows:

$$N_i(z) = \int_0^\infty P_i(z + \epsilon t) e^{-\lambda_i t} dt \quad (1)$$

Here $N_i(z)$ is the measured concentration of nuclide i (atoms g^{-1}) at depth z (g cm^{-2}), $P_i(z)$ is the production rate of nuclide i (atoms g^{-1} yr^{-1}) at depth z, λ_i is the decay constant of nuclide i (yr^{-1}), ϵ is the erosion rate (g cm^{-2} yr^{-1}), and t is time (yr), which is zero at the present time and positive for past times. If we have a prediction for the function $P_i(z)$, we can evaluate it by using this relationship to calculate the expected nuclide concentration at the sample depth and comparing it to the measured concentration. In simplified cases this can be solved directly for $P_i(z)$. For example, if $P_i(z)$ is assumed to be locally exponential in z with an e-folding length Λ, such that $P_i(z + \delta z) = P_i(z) \exp(-\delta z/\Lambda)$, then $P_i(z) = N_i(z)(\lambda_i + \epsilon/\Lambda)$ (also see discussion below). Alternatively, if the erosion rate is zero, then $P_i(z) = N_i(z)\lambda_i$ no matter what the form of $P_i(z)$.

The main difficulty with this approach is that it requires the assumption that the erosion rate has been steady for long enough for nuclide concentrations to reach a steady state in which nuclide production at given depth is balanced by radioactive decay and advection of material towards the surface by erosion. For ^{10}Be and erosion rates on the order of meters per million years, for example, this implies steady erosion for several million years, which is probably unlikely in nearly all real geological situations. As a practical matter, it is impossible to verify this assumption. However, one can mitigate the dependence on this assumption by looking for calibration sites with the lowest possible erosion rate. For one thing, this is useful because the lower the erosion rate, the higher the steady-state nuclide concentration, and thus the easier and the more precise the measurement. This is particularly important from the perspective of estimating subsurface production rates, because nuclide concentrations at several meters depth are orders of magnitude below those in surface samples. More importantly, the lower the erosion rate, the less sensitive the production rate estimate is to both the assumed value of the erosion rate and the assumption of steady erosion. A heuristic explanation for this is just that at very low erosion rates, nuclide concentrations are close to equilibrium between production and radioactive decay (the rate of which is known accurately). Thus, loss by erosion is a relatively small fraction of the nuclide balance, so uncertainty in the magnitude of loss by erosion has a commensurately small effect on the precision of the total production rate estimate. To show this quantitatively, simplify the production rate-depth relationship $P_i(z)$ as discussed above such that $P_i(z + \delta z) = P_i(z) \exp(-\delta z/\Lambda)$, where Λ is an e-folding length (g cm^{-2}). In this case (see Lal, 1991), Equation 1 is:

$$N_i(z) = \frac{P_i(z)}{\lambda_i + \frac{\epsilon}{\Lambda}} \tag{2}$$

Thus, one can compute $P_i(z)$from $N_i(z)$ by:

$$P_i(z) = N_i(z)\lambda_i + \frac{\epsilon N_i(z)}{\Lambda} \tag{3}$$

The (absolute) uncertainty in P_i, σ_P, that is derived from the (absolute) uncertainty in the erosion rate measurement σ_ϵ is:

$$\sigma_P = \sigma_\epsilon \frac{N_i(z)}{\Lambda} \tag{4}$$

where σ_ϵ is the uncertainty (g cm^{-2} yr^{-1}; here uncertainty is assumed to be Gaussian) in the erosion rate estimate. Given Λ = 1500 g cm^{-2} (appropriate for production by negative muon capture near ~1000 g cm^{-2} depth) and Λ = 4200 g cm^{-2} (appropriate for production by fast muons at greater depth), Figure 1 shows the relative uncertainty in the production rate estimate (that is, σ_P/P) resulting from a 50% uncertainty in the erosion rate estimate (that is, $\sigma_\epsilon = 0.5\epsilon$). At low erosion rates where nuclide loss by

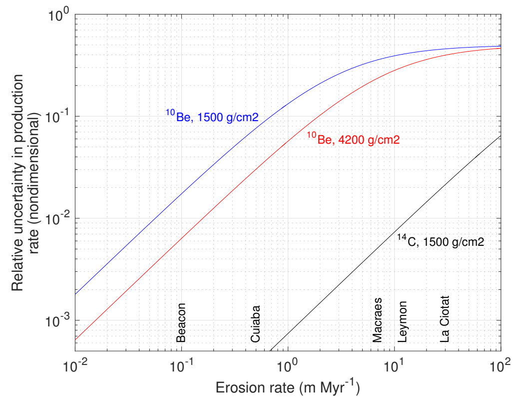

Figure 1: Relative uncertainty in production rate estimate (σ_P/P) for ^{10}Be resulting from a 50% uncertainty (that is, a relative uncertainty of 0.5) in the erosion rate estimate, for two different local e-folding lengths Λ (see text). Λ = 1500 g cm^{-2} approximates negative muon capture in the shallow subsurface (order 1000 g cm^{-2} depth), whereas 4200 g cm^{-2} approximates fast muon production at greater depths. In addition, the black line shows the equivalent result for ^{14}C with Λ = 1500 g cm^{-2}. Names of calibration sites discussed later in the text indicate erosion rates characteristic of each site. Rock density assumed 2.7 g cm^{3}.

radioactive decay is an important part of the nuclide balance, the uncertainty in estimating P_i is strongly dependent on the erosion rate, so lower erosion rate sites incur significantly lower uncertainties in production rate estimates. The uncertainty in estimating P_i also decreases for larger Λ, and the instantaneous value of Λ increases with increasing depth below the surface, so, for a given erosion rate, uncertainties in estimating the production rate will also decrease with increasing depth. The point of this exercise is that it shows that even if we relax our steady-state assumption to only the relatively weak assumption that the erosion rate has varied by less than 50% during the time period in which the nuclide concentrations accumulated, if we can find a site where the erosion rate is less than ca. 1 m Myr^{-1}, we can still estimate P_i with better than ca. 10% precision. If we can find a site where the erosion rate is less than ca. 10 cm Myr^{-1}, we can estimate production rates with percent-level accuracy. In addition, as shown in Figure 1, for a particular depth and erosion rate, uncertainty in estimating the production rate is smaller for nuclides with shorter half-lives. Thus, one could achieve desired precision in production rate estimates at higher erosion rates for ^{26}Al, ^{36}Cl, and particularly ^{14}C, than for ^{10}Be. To summarize, however, for the most accurate estimate of production rates due to muons, with minimal reliance on a strong steady-state assumption, we want calibration sites with the lowest possible erosion rates. One could also obtain the same effect by choosing deeper samples at a site with a higher erosion rate (I discuss this more later), but of course this would only permit accurate production estimates for some nuclides at large depths.

4.2. Existing calibration data sets

I will discuss published calibration data that are relevant to estimating muon production rates of ^{10}Be and ^{26}Al from five sites, as follows:

Beacon Heights, Antarctica. At this site, John Stone and colleagues collected a 25-m core in sandstone bedrock at 2183 m elevation in the McMurdo Dry Valleys of Antarctica. ^{10}Be and ^{26}Al measurements from this core by several laboratories are reported in Borchers et al. (2016). Surface nuclide concentrations at this site indicate an erosion rate near 0.1 m Myr^{-1}. This is by far the lowest erosion rate site for which calibration data exist. Balco et al. (2011b) reported ^{21}Ne measurements from this core, but I do not discuss them here.

La Ciotat, France. This site is a 10-m core in quartzose limestone bedrock at 310 m elevation. ^{10}Be and ^{26}Al (and also ^{36}Cl, which is not discussed further here) concentrations in this core are described by Braucher et al. (2011). Surface nuclide concentrations at this site indicate an erosion rate near 40 m Myr^{-1}.

Leymon quarry, Spain. This site consists of two 25-m cores (the ”Leymon Low” and ”Leymon High ” cores at 1246 and 1277 m elevation, respectively) drilled in a quartzite dike. Braucher et al. (2013) report ^{26}Al and ^{10}Be measurements for both cores, and Lupker et al. (2015) report *in-situ*-produced ^{14}C measurements for the Leymon High core. Surface nuclide concentrations here indicate erosion rates near 20 m Myr^{-1}.

Macraes Flat, New Zealand. This site is a series of mine excavations at 535 m elevation. Kim and Englert (2004) reported ^{10}Be and ^{26}Al measurements from samples up to ca. 180 m below the surface at this site. Although these authors concluded that near-surface nuclide concentrations were not in steady state with a constant erosion rate, subsurface nuclide concentrations indicate an erosion rate near 10 m Myr^{-1}. Although Kim et al. (2007) reported ^{14}C concentrations in quartz at this site, they concluded that a significant fraction of their observed concentrations was due to thermal neutron capture on N rather than muon interactions. Thus, I have not considered these measurements further.

Cuiaba, Brazil. This site consists of two open-pit excavations at 210 m elevation. ^{10}Be measurements from quartz veins at these sites are described by Braucher et al. (2003). Surface nuclide concentrations here indicate erosion rates on the order of 0.5-1 m Myr^{-1}.

Figures 2 and 3 show ^{10}Be and ^{26}Al data from these sites. I accept all mass depths of samples as reported in the source papers, with the exception that I independently carried out a depth adjustment for some samples at Cuiaba by fitting to a subsurface production profile, as described in section 6.2.1. The nuclide concentration measurements have been renormalized to common ^{10}Be and ^{26}Al measurement standards, as follows. For ^{10}Be, all measurements except those from Macraes Flat and Cuiaba were originally measured against ^{10}Be standards compatible with those of Nishiizumi et al. (2007). Those from Macraes Flat were measured against the ^{10}Be standards of Nishiizumi (2002) (R. Finkel, written communication), so have been corrected by a factor of 0.9042; those at Cuiaba were measured against the certified value of the NIST Be isotope ratio standard, so have been corrected by a factor of 1.042 (Nishiizumi et al., 2007). ^{26}Al measurements in these studies employed both the standards of Nishiizumi (2004) (measurements at LLNL-CAMS: all Macraes Flat and most Beacon Heights data) and those of Arnold et al. (2010) (measurements at ASTER: La Ciotat, Leymon Quarry, and some Beacon Heights data). ASTER ^{26}Al data have been normalized to the KNSTD standardization using a correction factor of 1.021, which is based on com-

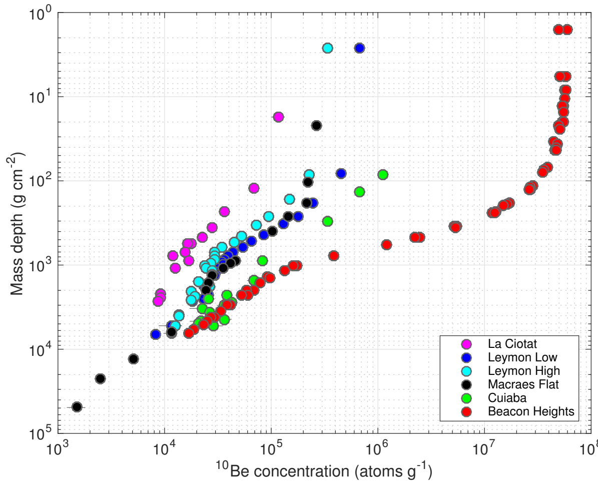

Figure 2: ^{10}Be calibration data from cores and excavations. All ^{10}Be concentration measurements have been normalized to the '07KNSTD' standardization as described in the text, but have not been otherwise corrected or adjusted; variation in nuclide concentrations among sites reflects variation in site elevation and erosion rate. Note that the depths of samples in the deeper of two excavations at Cuiaba have been adjusted using the fitting procedure described later in the text. Error bars show 1-σ uncertainties as reported in the source publications; where not shown they are smaller than the symbols used to plot the data at this scale.

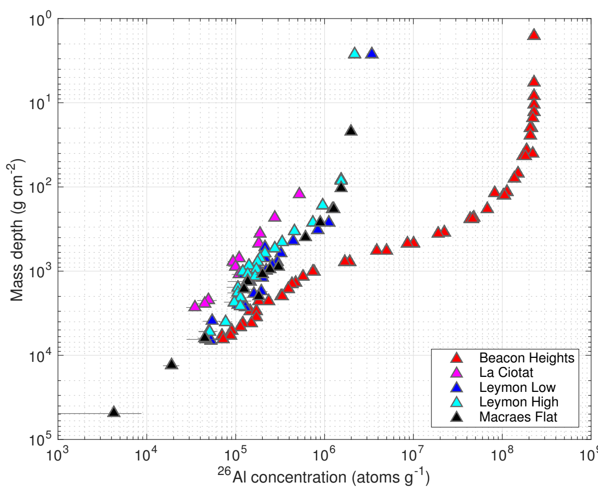

Figure 3: ^{26}Al calibration data from cores and excavations. All ^{26}Al measurements have been normalized to the 'KNSTD' standardization as described in the text. Error bars show 1-σ uncertainties as reported in the source publications; where not shown they are smaller than the symbols used to plot the data at this scale.

parison of the KNSTD Al standards with an Al standard derived from the same source material as the ASTER Al standards (Fink and Smith, 2007). Note that this renormalization of the ^{26}Al data has a minimal effect on any of the results in this paper.

5. Initial model calibration

I begin by fitting Models 1A and 1B to the data from the Beacon Heights core in order to obtain best estimates for muon interaction cross-sections. The reason to begin in this way is that this site has by far the lowest erosion rate, which, as discussed above, means that the parameter estimates will be least sensitive to both the accuracy of the erosion rate estimate from the surface nuclide concentration and the steady-erosion assumption. Borchers et al. (2016) estimated the erosion rate at Beacon Heights using the surface nuclide concentrations and spallogenic ^{10}Be and ^{26}Al production rate estimates derived from independent calibration data, and obtained a range of erosion rate estimates between 7-15 $\times$ 10^{-6} g cm^{-2} yr^{-1}.

These erosion rates expressed in linear rather than mass units are 2.5-5.5 cm Myr^{-1} given rock density of 2.7 g cm^{-3}. Note that throughout this paper I will use 2.7 g cm^{-3} as a standardized value for rock density in converting mass erosion rates in g cm^{-2} yr^{-1} to linear erosion rates in m Myr^{-1}, no matter what the actual density of the lithology in question (for example, the actual density of the sandstone at Beacon Heights is near 2.3 g cm^{-3}). Because mass erosion rates in g cm^{-2} yr^{-1} are used exclusively in all calculations in the paper, the value chosen for rock density has no impact on the calculations, and the conversion to linear units is only important as a means of representing erosion rates in more commonly used and more easily visualized units. Choosing a standard density for the conversion avoids potential confusion about whether surface erosion rates are computed for bedrock or soil densities, and simplifies comparisons of erosion rates observed at different sites.

The large range of the erosion rate estimates from the spallogenic inventory at Beacon Heights stems from differences in spallogenic production rate models. This is because a corollary to the observation above that a production rate estimate is insensitive to the assumed erosion rate when the erosion rate is low is that in the opposite situation, when one seeks to estimate the erosion rate from the surface nuclide concentration, a relatively small uncertainty in the production rate (in this case 10%) propagates into a large uncertainty in the erosion rate (in this case 50%). However, Figure 1 shows that a 50% uncertainty in the erosion rate, at an erosion rate of 3.5 cm Myr^{-1}, permits better than 1% precision on estimates of muon production rates at all depths. Thus, the steady-erosion assumption for this site contributes substantially less uncertainty to the production rate estimates than the measurement uncertainties ($>$ 3%). To summarize, the erosion rate at Beacon Heights is low enough that uncertainty in the absolute magnitude and steadiness of the erosion rate does not contribute significant uncertainty to estimates of muon production rates. In general, this is not the case for the other data sets, so I conclude that the Beacon Heights data will yield the most accurate calibration of muon interaction cross-sections or other fitted parameters. This, of course, was the purpose of collecting the Beacon Heights core in the first place.

I now describe the fitting procedure for models 1A and 1B (those based on the Heisinger muon flux calculations). Here I (i) rewrite Equation 1 to separate production by neutron spallation, negative muon capture, and fast muon interactions; (ii) represent spallogenic production by a single exponential in mass depth; and (iii) follow Heisinger in representing production by each of the two muon production pathways as the product of a cross-section or likelihood with a stopping rate or a flux. This yields:

$$N_i(z) = \frac{P_{sp,i}e^{-z/\Lambda_{sp}}}{\lambda_i + \frac{\epsilon}{\Lambda_{sp}}} + f_i^* \int_0^\infty R_{\mu^-}(z+\epsilon t) f_C f_d e^{-\lambda_i t} dt + \sigma_{0,i} \int_0^\infty \beta(z+\epsilon t)\Phi(z+\epsilon t)\bar{E}^\alpha(z+\epsilon t) N_i e^{-\lambda_i t} dt \quad (5)$$

In the first term, which describes spallogenic production, I take Λ_{sp} to be 140 g cm^{-2} for the Beacon Heights site (from Borchers et al., 2016) and ϵ to be 10×10^{-6} g cm^{-2} yr^{-1} (3.7 cm Myr^{-1}). As discussed above, for an erosion rate this low, estimates of muon interaction cross-sections are insensitive to the assumed value of the erosion rate; I duplicated the fitting exercise for erosion rates of 7 and 15×10^{-6} g cm^{-2} yr^{-1} and verified that this range of erosion rates contributes less than a 1% variation in the cross-section estimates. Given a prescribed value for ϵ, the integrals in the second term (describing production by negative muon capture) and the third term (describing production by fast muon interactions) are fully defined at any depth z by the Method 1A or 1B implementations of the Heisinger method (see the Heisinger papers for the definition of the symbols). This leaves the surface production rate of nuclide i due to spallation ($P_{sp,i}$; atoms g^{-1} yr^{-1}), a negative muon capture probability for nuclide i (f_i^*; dimensionless), and a fast muon interaction cross-section for nuclide i ($\sigma_{0,i}$; barns) as fitting parameters. Although we already have an estimate of $P_{sp,i}$ from Borchers, it is not as precise as their estimate of Λ_{sp}, so I retain it as a nuisance parameter to limit the effect of an inaccurate estimate of $P_{sp,i}$ on the muon interaction cross-sections. Also, for computational practicality, I limit the integration time to eight half-lives of the nuclide in question instead of infinity. To evaluate the integrals, I used the default numerical integration scheme in MATLAB R2015b. For Models 1A and 1B, an estimate of the mean atmospheric pressure at the surface is needed. Here I use the Antarctic pressure-elevation relationship of Stone (2000) to estimate this from the site elevation (2183 m elevation implies 741.8 hPa). For Model 1B I assume zero geomagnetic cutoff rigidity at the core site. To estimate best-fitting values of the free parameters, I minimized the chi-squared misfit between model and data, assuming reported measurement uncertainties for the nuclide concentrations and disregarding uncertainties in the mass depth of samples, and using the MATLAB implementation of the Nelder-Mead simplex search method.

Figure 4 shows the results of fitting Equation 5 to the ^{10}Be and ^{26}Al data from Beacon Heights using the Model 1A code described above, that is, the MATLAB implementation in Balco et al. (2008) of the Heisinger method. One aspect of the Heisinger method is that the fast muon interaction cross-section σ is assumed to increase with muon energy by a power law, such that if E is the muon energy, then $\sigma(E) = \sigma_0(E^\alpha)$, where σ_0 is the cross section for 1 GeV muons. Heisinger assumes α to be 0.75. Some recent work (Lifton et al., 2014, J. Stone, written communications) has suggested that the Heisinger method could be simplified without loss of accuracy by assuming $\alpha = 1$,

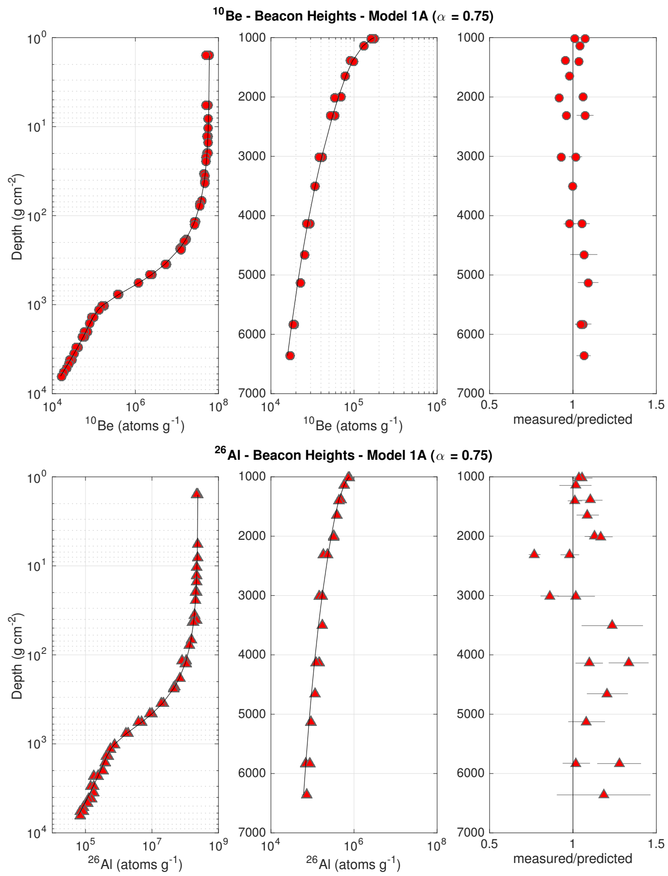

Figure 4: Fit of Model 1A with α = 0.75 to ^{10}Be (top) and ^{26}Al (bottom) measurements at Beacon Heights. Left panel shows all data on log-log axes; center panel shows data below 1000 g cm^{-2} depth on semilog axes; right panel shows model-data residuals as ratio of measured to predicted concentration for each sample. Error bars in right panel are 1σ measurement uncertainty as reported in the source papers.

that is, a linear energy dependence for σ. Thus, I also show in Figure 5 the results of fitting Model 1A to the Beacon Heights data with $\alpha = 1$. Figure 6 shows the results of fitting Model 1B, which uses the implementation of Heisinger in Lifton et al. (2014) as described above, to the Beacon Heights data. Note that Model 1B also assumes $\alpha = 1$.

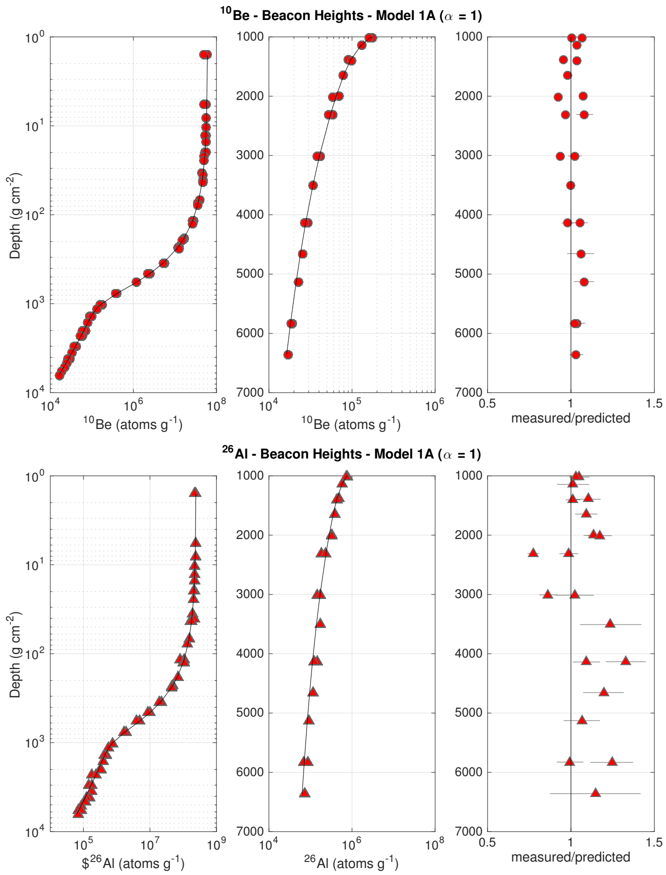

Figure 5: Fit of Model 1A with $\alpha = 1$ to ^{10}Be (top) and ^{26}Al (bottom) measurements at Beacon Heights. Left panel shows all data on log-log axes; center panel shows data below 1000 g cm^{-2} depth on semilog axes; right panel shows model-data residuals as ratio of measured to predicted concentration for each sample. Error bars in right panel are 1σ measurement uncertainty as reported in the source papers.

Table 1 shows best-fitting muon interaction cross-sections for Models 1A (with $\alpha = 0.75$ and $\alpha = 1$) and 1B. All fit the data similarly, as expected given that they are based on the same physics. The scatter of the observations around the model predictions in all cases substantially exceeds reported measurement uncertainties. In other words, if we assume that the sole source of uncertainty is the reported measurement uncertainty in the ^{10}Be and ^{26}Al concentrations, the probability-of-fit based on the chi-squared misfit is negligible, $< 1 \times 10^{-8}$ for either nuclide for any model. However, the

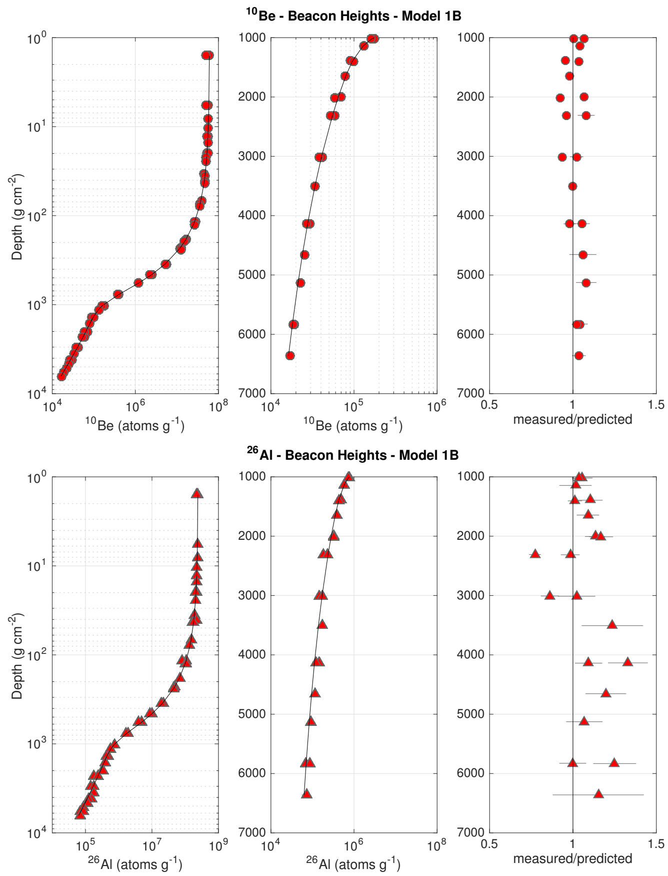

Figure 6: Fit of Model 1B to ^{10}Be (top) and ^{26}Al (bottom) measurements at Beacon Heights. Left panel shows all data on log-log axes; center panel shows data below 1000 g cm^{-2} depth on semilog axes; right panel shows model-data residuals as ratio of measured to predicted concentration for each sample. Error bars in right panel are 1σ measurement uncertainty as reported in the source papers.

distribution of residuals with respect to the model predictions is indistinguishable from normal, unbiased, and displays no obvious trend (Figures 4-6), which suggests that the main cause of scatter around the model predictions is unquantified measurement uncertainty rather than a systematic inaccuracy in the models. As the measurements from this core are from three different laboratories, this agrees with the conclusions of Jull et al. (2013) and Borchers et al. (2016) that measurement uncertainties for ^{10}Be and ^{26}Al reported by a particular laboratory underestimate true measurement uncertainties in an interlaboratory-comparison sense. Borchers et al. (2016) performed a similar fitting exercise to the Beacon Heights data using code similar to that of Model 1B but including expanded measurement uncertainties derived from the intercomparison of Jull et al. (2013), and found acceptable probabilities-of-fit; I accept this result and have not repeated this experiment here. Overall, these fitting exercises, as well as that of Borchers et al. (2016), show that Models 1A and 1B both fit the Beacon Heights data adequately. In addition, they indicate that simplifying the Heisinger method by setting $\alpha = 1$ has little effect on agreement with observations; in fact, scatter of data around model predictions is slightly (although not significantly) less for models with $\alpha = 1$ than for Model 1A with $\alpha = 0.75$ (Table 1). Henceforth in this paper, therefore, I assume $\alpha = 1$ when applying Model 1A.

The actual best-fitting values of f^* and σ_0 for Model 1A (with $\alpha = 1$) and Model 1B are similar to those obtained by Borchers et al. (2016), which, as noted above, used code similar to Model 1B. As has been pointed out by numerous others previously (e.g., Balco et al., 2008; Braucher et al., 2003, 2011, 2013), the cross-section estimates for ^{10}Be and ^{26}Al derived from fitting to available geological calibration data are ~50% lower than the direct laboratory measurements of the cross-sections by irradiation of synthetic mineral targets by high-energy muons reported by Heisinger (Table 1). In other words, Heisinger's cross-section measurements overestimate observed ^{10}Be and ^{26}Al concentrations in this core by approximately a factor of two. Although it has been proposed that this mismatch may be related to Heisinger's choice of a value for α in scaling laboratory measurements of the fast muon interaction cross-section made at high energy down to typical muon energies at moderate depths, this cannot fully account for the mismatch. If, for example, one were to assume $\alpha \simeq 1.3$, this could reconcile estimates of σ, but not f^*.

To summarize, muon production rates calculated using models based on Heisinger's method with fitted muon interaction cross-sections successfully match ^{26}Al and ^{10}Be concentrations in the Beacon Heights deep core. This is a relatively stringent test because the erosion rate is low enough that the comparison is insensitive to uncertainties in the geological history of the site. However, calibrated values of f^* and σ_0 necessary to achieve this agreement are approximately 50% lower than values of the same parameters measured by Heisinger in irradiation experiments. For the purposes of this paper, this is interesting but not directly relevant: the aim here is not to figure out what happened in Heisinger's experiments, but to accurately estimate production rates in geologically useful settings. The fitting exercise shows that this can be accomplished with the calibrated cross-section estimates.

I now turn to estimating the uncertainty in the production rate estimates. Note that for the purposes of this paper, the uncertainties in the cross-section estimates themselves are not of interest, because I am not interested in what the actual values of these parameters are. Rather, I am interested in the uncertainties in estimates of production rates based on best-fitting values of these parameters. Thus, I have not attempted to compute an uncertainty in the cross-section estimates. Potentially, one can estimate the uncertainty in model-predicted muon production rates by computing the scatter of the residuals between predictions and observations for the calibration data. For data from deeper than 1000 g cm^{-1} where spallogenic production is negligible, this scatter for both Models 1A and 1B is ∼5% for ^{10}Be and ∼12% for ^{26}Al (Table 1). This only slightly exceeds the estimates of Borchers et al. (2016) for total measurement uncertainty in ^{10}Be and ^{26}Al of 3.6% and 10.1%, respectively, for low concentrations representative of the deep samples at this site. Thus, as also noted by Borchers et al. (2016) and already mentioned above, nearly all of the observed scatter around model predictions is due to measurement uncertainty. Remaining differences between model predictions and observations could, potentially, be due to (i) uncertainties in mass depth estimates for the samples; (ii) possible changes in the erosion rate in the past, or (iii) inaccuracies in the models. If we assume that of the observed 5% model-data scatter for ^{10}Be, 3.6% is contributed by measurement uncertainty, this leaves a potential 3% uncertainty due to these three factors. Thus, I conclude that uncertainty in muon production rates estimated by Models 1A and 1B at Beacon Heights that derives from the models themselves is less than 3%. Note that this does not include any uncertainty associated with scaling muon production rates from Beacon Heights to other locations. I discuss that in the next section.

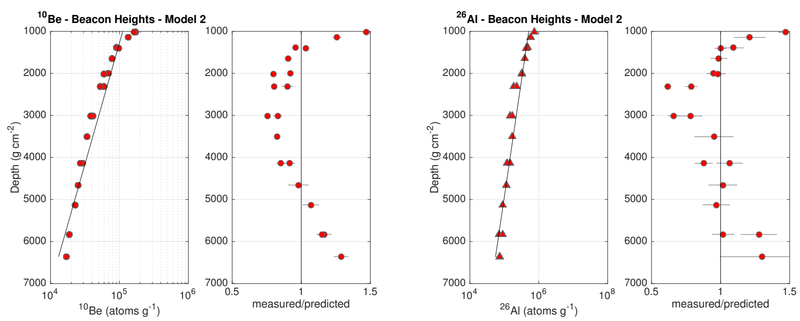

Figure 7: Fit of Model 2 to ^{10}Be (left 2 panels) and ^{26}Al (right two panels) measurements at Beacon Heights. Left panel of each pair shows data below 1000 g cm^{-2} depth on semilog axes; right panel of each pair shows model-data residuals as ratio of measured to predicted concentration for each sample. Error bars in right panel are 1σ measurement uncertainty as reported in the source papers.

Finally, I evaluate the exponential-approximation model for muon production rates by fitting a single exponential function in depth, as proposed by various authors and denoted 'Model 2' above, to the Beacon Heights data. Following the procedure given in Braucher et al. (2013), I fit the equation $N_i(z) = N_{0,i} \exp(-\Lambda_{\mu,i}/z)$ to all data below 1000 g cm^{-2} depth. This yields best-fitting values of a surface concentration of muon-produced nuclides $N_{0,i}$ (atoms g^{-1} yr^{-1}) and an effective e-folding length $\Lambda_{\mu,i}$ (g cm^{-2}). The concentration $N_{0,i}$ can then be related to a surface production rate due to muons $P_{0,i}$ using the relationship $P_{0,i} = N_{0,i}/(\lambda_i + \epsilon/\Lambda_{\mu,i})$ and an estimate of ϵ obtained from the surface spallogenic nuclide inventory.

Figure 7 shows the result of fitting this model to the Beacon Heights data. It is evident from this figure that this model is not adequate for fitting these data: a systematic trend in the residuals, in which the model overestimates nuclide concentrations at middle depths and underestimates them at the top and bottom of the core, is present both for ^{10}Be and ^{26}Al. In other words, a single exponential function fit to all data has too long an e-folding length to fit the shallow data, and too short an e-folding length to fit the deep data. This form of misfit is expected from the basic physics of muon production. Because the muon energy spectrum becomes more energetic with depth, the instantaneous e-folding length of the production rate increases commensurately, and this effect is not captured by a single exponential function. In addition, the e-folding length $\Lambda_{\mu,i}$ obtained from fitting to the Beacon Heights data (2500 g cm^{-2}; Table 1; Figure 7) is substantially lower than values of 4000-5000 g cm^{-2} obtained by Braucher et al. (2013) from fitting to data from other sites. The primary reason for this difference, and in addition the primary reason that the systematic misfit between the exponential model and observations that is obvious at Beacon Heights is less evident in the data considered by Braucher et al. (2013), is because that work considered data from sites with erosion rates that are at one to two orders of magnitude higher than the erosion rate at Beacon Heights. Heuristically, the effect of increasing the erosion rate is to increase the apparent e-folding length of the depth-concentration profile at a particular depth by ”dragging” the lower part of the profile up and increasing the importance of the fast muon contribution (which has a longer e-folding length) at the expense of the negative muon capture contribution (which has a shorter e-folding length). Thus, for a site with a faster erosion rate, the depth-concentration profile conforms more closely to that expected for fast muon production alone in that it displays an e-folding length that is both longer and changes less rapidly with depth than would be the case for a site with a slower erosion rate. The performance of an exponential approximation in matching measured concentrations will therefore improve with increasing erosion rate.

In Figure 8 I demonstrate this effect by computing expected concentrations of muon-produced nuclides at moderate depths using Model 1A and then fitting them with a single exponential function. In addition to the inverse relationship between erosion rate and fitted e-folding length for an exponential approximation noted above, fitted e-folding lengths are shorter at higher elevation, because production from stopped negative muons (which has a shorter e-folding length) increases more rapidly with elevation than production from fast muon interactions (which has a longer e-folding length). This calculation correctly predicts fitted e-folding lengths in the 4000-5000 g cm^{-2} range observed in the compilation by Braucher et al. (2013) at low elevations and erosion rates of order 10 m Myr^{-1}, as well as the apparent e-folding length near 2500 g cm^{-2} observed at Beacon Heights (Figure 7). Note, however, that it does not explain the apparent e-folding length near ~5000 g cm^{-2} for ^{10}Be concentrations measured at Cuiaba (Braucher et al., 2013); an apparent e-folding length closer to 3500 g cm^{-2} is expected for the relatively low erosion rate at that site. This mismatch may be a consequence of the relatively high measurement scatter at that site, but it is otherwise unexplained. It would be useful to revisit this issue by additional measurements at a similar low-erosion-rate site at low elevation.

To summarize, the measurements at Beacon Heights, where the erosion rate is ex-

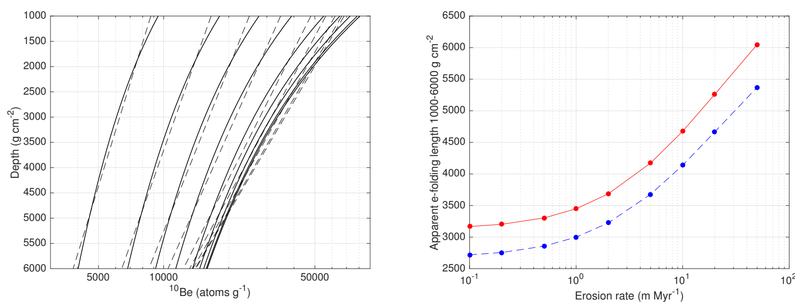

Figure 8: Calculation of apparent e-folding lengths for muon-produced ^{10}Be concentrations as a function of erosion rate and elevation. This calculation uses Model 1A (with $\alpha = 1$) to predict steady-state nuclide concentrations between 1000-6000 g cm^{-2} for a range of erosion rates, then fits an exponential function to the calculated nuclide concentrations in the same way as is shown for the Beacon Heights data in Figure 7 above. The left panel shows depth-concentration profiles for a range of erosion rates between 0.1-50 m Myr^{-1} calculated with Model 1A as solid lines, with corresponding best-fitting exponential approximations as dashed lines. Higher erosion rates predict lower concentrations, so curves for higher erosion rates are at left in this figure. For higher erosion rates the contribution of negative muon capture production is less, which results in a longer apparent e-folding length and a closer match to an exponential approximation. At lower erosion rates, the contribution of negative muon capture production is greater, the apparent e-folding length is shorter, and the divergence between actual concentrations and the exponential approximation will be greater. The right-hand panel shows fitted e-folding lengths (that is, the slopes in semilog space of the red-lines in the left-hand figure) as a function of erosion rate. The red line shows results for 1013.25 hPa (sea level); blue dashed line is for 750 hPa (similar to the Beacon Heights site).

tremely low, highlight that an exponential approximation for muon production oversimplifies the actual depth-dependence of muon production rates. A simplified exponential model is not expected, based on theoretical considerations, to accurately predict muon production rates or, therefore, to accurately predict concentrations of muon-produced nuclides across a wide range in erosion rates. Observations at Beacon Heights agree with this expectation. However, it is equally important to note that sites with an erosion rate this low are extremely rare on Earth, so it is highly likely, as pointed out by Braucher et al. (2013) and many others, that the exponential model can potentially provide an acceptably accurate and very much simpler method of estimating concentrations of muon-produced nuclides for many geological applications. I explore that in more detail later in the paper.

6. Geographic scaling

The previous section described fitting Models 1A and 1B to data from the Beacon Heights core and showed that both these models can be adequately fit to the observations. I now ask whether these models, which both include a geographic scaling method for the surface muon spectrum, are effective at scaling muon production rates from the calibration site at Beacon Heights to other locations.

I will not further discuss Model 2 (the single-exponential model) in this section, because, as discussed above, it is evident from a comparison of Figures 7 and 8 above with the results of Braucher et al. (2013) that Model 2 with parameters calibrated from Beacon Heights will perform poorly at other bedrock core sites with different erosion rates. The fitted e-folding length for subsurface nuclide concentrations at Beacon Heights (2500 g cm^{-2}; see Table 1) is very different from that observed at La Ciotat and Leymon Quarry (4000-5000 g cm^{-2}; see Table 2 of Braucher et al., 2013), so an exponential model derived from the former would clearly not fit the latter. Thus, I have not carried out this exercise. I return to the question of when a simplified exponential model can be used with acceptable accuracy for geological applications later in the paper.

6.1. Bedrock core data at relatively high-erosion-rate sites

Ideally, one could test geographic scaling models by calibrating the models at one location with an extremely low erosion rate (e.g., Beacon Heights), using the calibrated models to predict nuclide concentrations at a different site with an equally low erosion rate, and comparing these predictions to measurements at the new site. If the erosion rate at the new site were low enough, we would not need an accurate estimate of the erosion rate. However, other sites where data from deep bedrock cores are available (La Ciotat and Leymon Quarry) have surface erosion rates (inferred from spallogenic nuclide concentrations in surface samples) that are two orders of magnitude higher, in the 10-40 m Myr^{-1} range. At these erosion rates, as discussed above and shown in Figure 1, the concentration of muon-produced nuclides has a strong dependence on the erosion rate. At these higher-erosion-rate sites, we can estimate the steady-state erosion rate from the spallogenic nuclide concentration and use that erosion rate with a muon production model to predict concentrations of muon-produced nuclides in the subsurface for comparison with observations. However, the results of this comparison are very dependent on the steady-erosion assumption, because if the erosion rate changed over time, the spallogenic nuclide inventory would reach equilibrium with a new erosion rate faster than the muon-produced inventory. In this case, there would be no single value for a steady-state erosion rate that could successfully predict both spallogenic nuclide concentrations in near-surface samples and muon-induced nuclide concentrations in deeper samples. We could, therefore, observe a mismatch between predicted and measured concentrations of muon-produced nuclides either because (i) the muon production rate scaling model is incorrect, or (ii) the scaling model is correct, but our assumption that both spallogenic and muon-produced nuclide inventories are in equilibrium with the same steady erosion rate is incorrect. In practice, there is no way to independently verify the steady-state assumption, which then implies that we can not evaluate the scaling model with high confidence either. In fact, one could argue that the steady-state assumption is likely to be false because all the sites have experienced periodic climate change, which presumably affected erosion rates at least to some extent, during the Pleistocene (see Braucher et al., 2003, for a more detailed discussion of this effect).

Despite the difficulty of differentiating the performance of muon production models from the validity of the steady state assumption at these sites, this test is still potentially useful, because one might find that the muon scaling models calibrated at Beacon Heights were not able to successfully predict observed concentrations of muon-produced nuclides at the other core sites for any erosion rate. If the production model could not successfully predict observed nuclide concentrations for any value of the erosion rate, this would show that the model is incorrect. In other words, although it is not possible to prove unambiguously that a scaling model is correct, it might be possible to show that it is incorrect. Thus, in this section I carry out this comparison exercise for the La Ciotat, Leymon Low, and Leymon High cores. I address the data from excavations at Cuiaba and Macraes Flat in the next section. Here I am fitting the following equation to the ^{26}Al and ^{10}Be data (separately) at each site:

$$N_i(z) = N_{sp}e^{-\frac{z}{\Lambda_{sp}}} + f_i^* \int_0^\infty R_{\mu^-}(z+\epsilon t) f_C f_d e^{-\lambda_i t} dt + \sigma_{0,i} \int_0^\infty \beta(z+\epsilon t)\Phi(z+\epsilon t)\bar{E}^\alpha(z+\epsilon t) N_i e^{-\lambda_i t} dt \quad (6)$$

This is the same as Equation 5 except that the spallogenic nuclide inventory, which is defined as a function of the erosion rate in Equation 5, is represented here by a single parameter N_{sp} with units of atoms g^{-1}. The muon interaction cross-sections f_i^* and $\sigma_{0,i}$ are known from fitting each model to the Beacon Heights data as described above, and the parameter Λ_{sp} is obtained for the elevation and magnetic cutoff rigidity of each site using the table of Marrero et al. (2016) (magnetic cutoff rigidity is estimated from the geographic latitude of the site using the equation in Lifton et al., 2014). This leaves the erosion rate ϵ and the spallogenic nuclide inventory at the surface N_{sp} as the fitting parameters. Subsequently, given an (independent) estimate of the nuclide production rate due to spallation (P_{sp}) at the site, one can then interpret N_{sp} as an apparent steady-state erosion rate implied by the spallogenic nuclide inventory ϵ_{sp} using the relationship $N_{sp} = P_{sp}/(\lambda + \epsilon_{sp}/\Lambda_{sp})$. Basically, the purpose of this procedure is to make two estimates of the steady-state erosion rate at each site independently from the spallogenic and muon-produced nuclide inventories. I then consider (i) whether the muon scaling model can fit the measurements for any value of the erosion rate, and (ii) whether estimates of the erosion rate from spallogenic and muon-produced nuclide concentrations agree. As discussed above, agreement between the two erosion rate estimates would, in a general sense, indicate that the muon production model is successful at scaling muon production rates between sites, but disagreement between the estimates could mean either that the production model fails or that the steady-state erosion assumption fails. In other words, a failure to fit the data at any erosion rate could falsify the hypothesis that a muon scaling model is correct, but success in fitting the data would not prove the hypothesis. Other details of the fitting procedure here are as follows. Following the discussion above, in this section I will only consider the case where $\alpha = 1$ for both Model 1A and Model 1B. I estimate the atmospheric pressure at each site using the ERA40 atmosphere as implemented by Lifton et al. (2014). To compute spallogenic production rates necessary for interpreting the best-fitting spallogenic inventory N_{sp} as an erosion rate, I use the 'St' scaling method and production rate calibration of Borchers et al. (2016).

Figures 9 and 10 show the results of this fitting exercise. Scatter around the best-fitting models at most sites is greater than observed at Beacon Heights (Table 2), but no systematic bias to the residuals is evident. Model 1A displays slightly less scatter

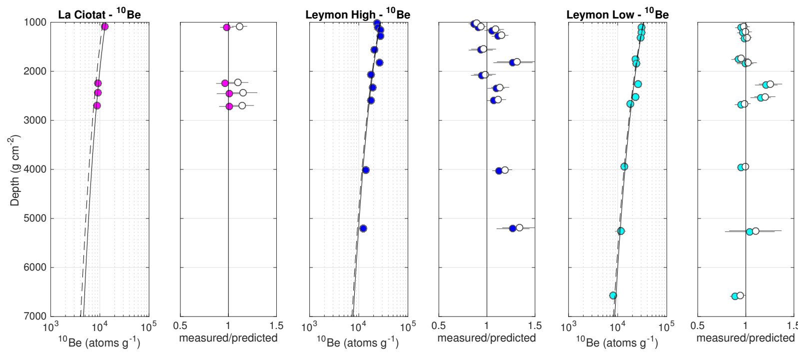

Figure 9: Best fit of Models 1A (with α = 1) and 1B, with cross-sections calibrated to the Beacon Heights data, to ^{10}Be measurements for La Ciotat and Leymon Quarry bedrock cores. Left panel of each pair shows data below 1000 g cm^{-2} depth on semilog axes with best-fitting predicted nuclide concentrations for Model 1A (solid line) and 1B (dashed line). Right panel of each pair shows model-data residuals as ratio of measured to predicted concentration for each sample: solid symbols are for Model 1A and open symbols for Model 1B. Error bars in right panel are 1σ measurement uncertainty as reported in the source publications. Although only the data below 1000 g cm^{-2} are shown here, the models were fit to all data.

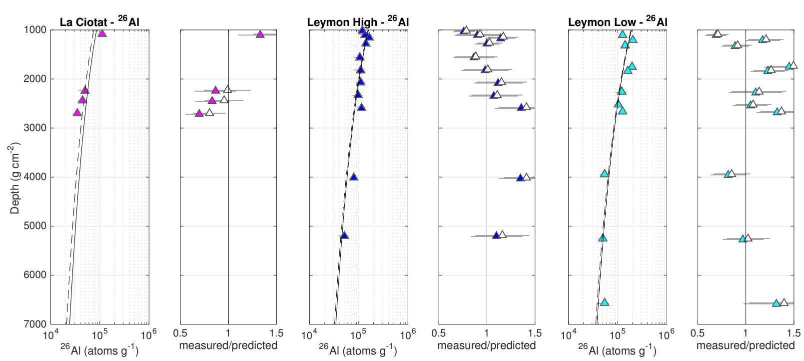

Figure 10: Best fit of Models 1A (with α = 1) and 1B, with cross-sections calibrated to the Beacon Heights data, to ^{26}Al measurements for La Ciotat and Leymon Quarry bedrock cores. Axes and symbols are the same as for Figure 9.

with respect to the observations than Model 1B in all cases, but the differences are not significant.

Table 2 shows apparent steady-state erosion rates inferred from spallogenic and muon-produced nuclide inventories for ^{26}Al and ^{10}Be for these three sites. At La Ciotat, erosion rate estimates from the muon-produced inventory for ^{26}Al and ^{10}Be and for both models (27-33 m Myr^{-1}) are substantially (~50%) higher than the erosion rate estimated from the spallogenic inventory (18-21 m Myr^{-1}). As noted above, this difference could be explained either by a failure of the muon production scaling or by the fact that the site has not experienced steady erosion; it is not possible to determine which from these data alone.

At the Leymon High site, on the other hand, erosion rate estimates from the muon-produced inventory (12-14 m Myr^{-1}) are lower, although not significantly so, than erosion rate estimates from the spallogenic inventory (17 m Myr^{-1}). At the Leymon Low site, the two estimates are similar (8-13 m Myr^{-1}). The agreement between erosion rate estimates from spallogenic and muon-produced inventories at this site is consistent with the hypothesis that (i) nuclide concentrations have reached steady state with the erosion rate and also (ii) the muon scaling models are correct. However, again, it is not possible to exclude the possibility that both parts of the hypothesis are incorrect in such a way as to produce spurious agreement between the erosion rate estimates.

To summarize, it is possible to find erosion rates that provide a good fit to core data at La Ciotat and Leymon Quarry using either Model 1A or 1B calibrated with the Beacon Heights data. Thus, these data provide no evidence that either of these models is incorrect or inaccurate. However, because of the ambiguity regarding whether poor agreement between steady erosion models inferred from spallogenic and muon-produced nuclides indicates a failure of the scaling model or a failure of the steady-state assumption, it is not possible to evaluate the performance of the scaling models any more precisely than this with these data. In general, however, results from these three core sites show better agreement between apparent erosion rates derived from muon-produced and spallogenic nuclide inventories at lower-erosion-rate sites. This would tend to indicate that mismatches between erosion rate estimates are more likely caused by non-steady-state erosion than by errors in muon production rate scaling. To summarize, data from these bedrock cores are consistent with, although they do not prove, the hypothesis that both Model 1A and 1B are accurate for scaling muon production rates from Beacon Heights to these sites.

6.2. Other sites with lower erosion rates

Two other sites not discussed in the previous section, Macraes Flat and Cuiaba, are potentially more useful for testing the geographic scaling in Models 1A and 1B because these sites are deeper (Macraes Flat) or have a lower erosion rate (Cuiaba) than the La Ciotat or Leymon Quarry sites. Both of those factors reduce the dependence of the muon-produced nuclide concentrations on the erosion rate. Thus, we can use some data from these sites to test the muon scaling models with less reliance on the assumption that spallogenic and muon-produced erosion rates are in equilibrium with the same steady erosion rate. The Cuiaba site is potentially particularly useful for this, because its low-elevation, low-latitude location maximizes the difference in production rate scaling relative to the Beacon Heights site. On the other hand, both Macraes Flat and Cuiaba are geomorphically more complicated than the bedrock core sites. In both cases, samples were collected opportunistically from existing mining excavations, and a number of assumptions about the mass thickness of material removed during various stages of mine site preparation, etc., were required to estimate the sample depths below the surface. This contributes some uncertainty to using these measurements as calibration data.

6.2.1. Cuiaba

At Cuiaba, Braucher et al. (2003) collected samples from two sites: a deep open-pit excavation where the original soil surface was not present and the amount of pre-stripping prior to excavation was not exactly known; and a second site, in a different location from the main excavation, where the original soil surface was present but only a shallow excavation could be made. This situation creates two potential uncertainties: first, in reconstructing the thickness of soil originally present at the deep site; second, in the assumption that the erosion rate is the same at both sites. These authors inferred the original depth of the deep samples by comparing measured ^{10}Be concentrations at both sites and choosing an original soil thickness at the deep site that was consistent with nearby observations from undisturbed soils and also yielded a continuous nuclide concentration profile when data from both sites were considered together. I use a similar strategy here. First, I fit Equation 6 to the ^{10}Be measurements from both sites, with the original cover thickness above the deep site as an additional free parameter. This yielded a best-fitting cover thickness of 1490 g cm^{-2} (for Model 1A with $\alpha = 1$), which is similar to the results of Braucher et al. (2003) (although this value is only stated as "about 4 m" in the paper, examination of their Figure 2 indicates it is near 1200 g cm^{-2}), and a steady erosion rate near 0.5 m Myr^{-1}. Second, using this value of the cover thickness, I compare the measurements to predicted ^{10}Be concentrations for a range of erosion rates spanning an order of magnitude between 0.2-2 m Myr^{-1} using Models 1A and 1B.

Figure 11 shows this comparison. Although the measurements at this site are somewhat scattered, if we accept that nuclide concentrations at the site have, in fact, reached equilibrium with a steady erosion rate somewhere in the range 0.2-2 m Myr^{-1}, ^{10}Be concentrations predicted by Model 1A (with $\alpha = 1$) for this range of erosion rates are consistent with the observations in that there is no significant systematic residual between observations and predictions. However, concentrations predicted by Model 1B systematically underestimate the observed concentrations for any erosion rate. This would imply that the geographic scaling of muon fluxes in Model 1B overestimates the difference in subsurface muon flux between Beacon Heights and Cuiaba. Note that the mismatch between Model 1B and the observations cannot be explained by a potential inconsistency in using Model 1A to estimate the original soil thickness at the deep site: the soil thickness would have to be less than 500 g cm^{-2} to explain the mismatch, which appears inconsistent with the authors' observations as described in the paper. A failure of the steady-erosion assumption could not explain it either, because the observed concentrations are systematically higher than Model 1B would predict even for zero erosion at this site. To summarize, although the difficulty in estimating the original configuration of the site creates some uncertainties in this conclusion, this comparison between model predictions and the obervations at Cuiaba indicates that the

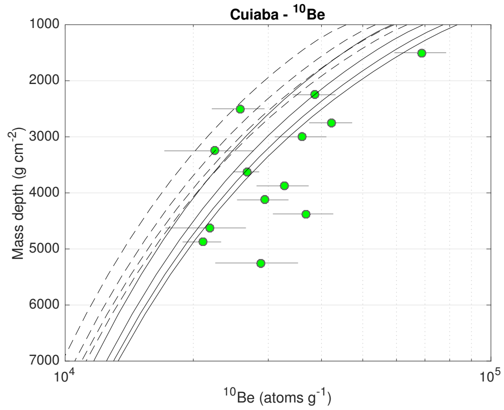

Figure 11: Comparison of ^{10}Be concentrations at Cuiaba site with those predicted by Models 1A (with α = 1; solid lines) and 1B (dashed lines), with cross-sections calibrated to the Beacon Heights data as described above, for a range of erosion rates. Lines correspond to erosion rates of 0.2 (rightmost), 0.5, 1, and 2 (leftmost) m Myr^{-1}. Error bars show 1σ uncertainties as reported in the source paper.

simpler elevation scaling of the muon flux in Model 1A is more accurate than the more complicated geographic scaling of Model 1B in scaling production rates calibrated at Beacon Heights to this low-elevation, low-latitude site.

6.2.2. Macraes Flat

At Macraes Flat, the likely erosion rate is higher, but samples were collected from deeper below the surface. Fitting Equation 6 to subsurface data with either Model 1A or 1B yielded erosion rate estimates of 5-10 m Myr^{-1}, in approximate agreement with the estimate of 12 m Myr^{-1} by Kim and Englert (2004). This site is composed of several distinct excavations, each of which represents a different, non-overlapping, range of depths below the original surface. In addition, these authors concluded from both geomorphic criteria and the observations themselves that the near-surface concentrations are not in equilibrium with steady erosion. However, nuclide concentrations in samples from the deepest site ($>$ 10,000 g cm^{-2}) are relatively insensitive both to the steady-erosion assumption and to potential inaccuracies in estimating the original land surface configuration. Thus, I carried out an analysis similar to that described above for the Cuiaba site for these deepest samples.

Figure 12 shows the results. Predictions for a range of erosion rates between 2 and 20 m Myr^{-1} are consistent with ^{10}Be and ^{26}Al measurements between 10,000-25,000 g cm^{-2} depth. However, the deepest ^{10}Be measurement at 50,000 g cm^{-2} depth is almost double the concentration predicted at that depth by either scaling model. The significance of the failure to fit with the deepest ^{10}Be measurement is unclear; the only way to reconcile this measurement with the ^{10}Be concentrations in the overlying samples would be if α was substantially greater than 1, which would be inconsistent with other calibration data as well as with laboratory measurements. It would probably be valuable to replicate this ^{10}Be measurement. The corresponding ^{26}Al measurement is not

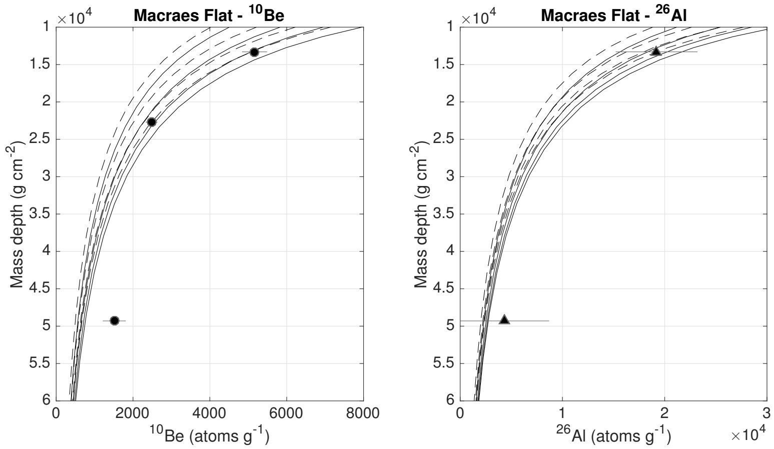

Figure 12: Comparison of ^{10}Be and ^{26}Al concentrations at Macraes Flat with those predicted by Models 1A (with $\alpha = 1$; solid lines) and 1B (dashed lines), with cross-sections calibrated to the Beacon Heights data as described above, for a range of erosion rates. Error bars show 1σ uncertainties as reported in the source paper. Lines correspond to erosion rates of 2 (rightmost), 5, 10, and 20 (leftmost) m Myr^{-1}.

similarly anomalous, although it has relatively large measurement uncertainty. Model 1A and 1B predictions are very similar at this site; both can explain the measurements in the 10,000-25,000 g cm^{-2} depth range given an erosion rate in the range 2-20 m Myr^{-1}.

6.3. Summary: geographic scaling of muon production rates

In the previous section I calibrated muon production models using data from the lowest-erosion-rate site available at Beacon Heights. In this section, I carried out a series of tests to determine whether the calibrated models can successfully account for ^{10}Be and ^{26}Al concentrations in subsurface calibration samples elsewhere. The only significant difference in the performance of model 1A and 1B is that Model 1B appears to overestimate the difference in production rate scaling between the high-elevation, high-latitude (e.g., low geomagnetic cutoff rigidity) at Beacon Heights and the low-elevation, low-latitude (high cutoff rigidity) site at Cuiaba. At all other sites, both models 1A and 1B are successful in matching observations.

7. Muon production of ^{14}C in quartz

For completeness and to facilitate use of Models 1A and 1B to compute ^{14}C production rates due to muons, I also fit Models 1A and 1B to measurements of *in-situ*-produced ^{14}C in quartz in the Leymon High core described by Lupker et al. (2015), using a similar approach as described above for fitting production models to ^{26}Al and ^{10}Be measurements in the Beacon Heights core. Although the erosion rate is much higher at the Leymon High site (10-15 m Myr^{-1}; see Table 2), the short half-life of

^{14}C improves the precision of production rate estimates for a given erosion rate by two orders of magnitude relative to ^{10}Be or ^{26}Al. The analysis shown in Figure 1, if applied to ^{14}C measurements, shows that the expected uncertainty in calibrating muon production models for ^{14}C at the Leymon High core is similar to that in calibrating production models for ^{26}Al and ^{10}Be at Beacon Heights.

The limited depth range of the ^{14}C measurements at the Leymon High core, as noted by Lupker et al. (2015), means that these data provide very little resolving power on the fast muon interaction cross-section σ_0, so it is only possible to accurately estimate the negative muon capture probability f^*_{14}. Thus, I fit Equation 5 to the ^{14}C measurements by assuming that the erosion rate is 12 m Myr^{-1} as inferred from ^{10}Be and ^{26}Al concentrations, assuming Λ_{sp} = 160 g cm^2 (Lupker et al., 2015), and assuming the experimentally determined value of σ_0 from Heisinger et al. (2002b, ; 2.4 μb for α = 1). This leaves two free parameters: f^*_{14} and a production rate due to spallation P_{sp}, which is a nuisance parameter for the present purpose.

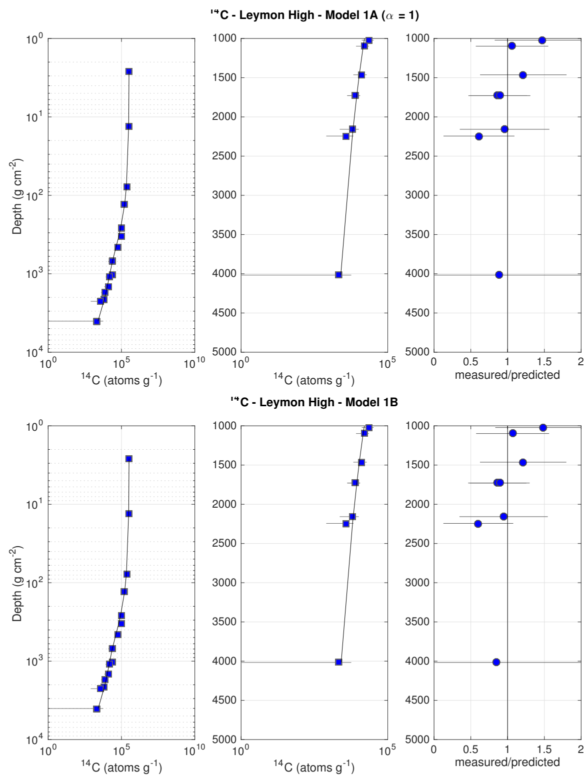

Figure 13: Fit of Model 1A with α = 1 (top) and Model 1B (bottom) to ^{14}C measurements at Leymon High core. Left panels show all data on log-log axes; center panels show data below 1000 g cm^{-2} depth on semilog axes; right panels show model-data residuals as ratio of measured to predicted concentration for each sample. Error bars are 1σ 'total' uncertainties of Lupker et al. (2015).

Figure 13 shows the results of this fitting exercise. This yields best-fitting values for f^*_{14} of 0.116 (Model 1A) and 0.114 (Model 1B). This closely replicates the results of a similar fitting exercise by Lupker et al. (2015), although they used slightly different code to compute the muon fluxes and in addition allowed σ_0 to float in their calculation, and obtained a slightly different best-fitting value as a result (0.134). As also noted by these authors, all these estimates are in much better agreement with the experimentally determined value of Heisinger (0.137) than is the case for ^{10}Be or ^{26}Al.

8. Needed accuracy/precision for burial-dating applications.

The previous sections show that, as expected from theoretical considerations, relatively complicated methods for estimating subsurface production rates that are based on downward propagation of the surface muon flux perform better at matching available calibration data than simplified exponential approximations. In this and subsequent sections, I discuss to what extent this difference is important for various geological applications that require computing production rates due to muons.

First, I consider the related applications of burial dating and depth profile dating. Burial dating relies on measurements of pairs of cosmic-ray-produced nuclides that are produced in a fixed ratio during surface exposure, but have different half-lives (see Granger, 2006, for a review). In a sample that is exposed at the surface, the ratio of these nuclides will conform to the production ratio. If the sample is then buried so that it is shielded from the cosmic-ray flux, the two nuclides will decay at different rates, so their ratio will be related to the duration of burial. Although this basic concept does not inherently require one to compute subsurface production rates due to muons, in many practical applications of this method samples are buried at relatively shallow depths, so nuclide production continues after burial, although at a lower rate than at the surface. In this case, determining the burial age of the sample requires an estimate of the production rate due to muons at the depth the samples are buried, and the accuracy of this estimate of the subsurface production rate has a significant effect on the accuracy of the eventual burial age. How important this effect is depends on the relationship of the total nuclide concentrations to the subsurface production rates. It is relatively unimportant if the sample was buried deeply with a high nuclide concentration and/or has been buried for a short time; it is very important if the sample has been buried for a long time at a shallow depth, so that the measured nuclide concentrations are predominantly the result of post-burial production.

Depth profile dating is an approach aimed at determining both the exposure age and erosion rate of landforms that have eroded after their initial emplacement (e.g., see summary in Hidy et al., 2010). It relies on the fact that the spallogenic nuclide inventory near the surface of an eroding landform is strongly dependent on the erosion rate, and weakly dependent on the exposure age, whereas the muon-produced nuclide inventory at several meters depth is weakly dependent on the surface erosion rate and strongly dependent on the exposure age. Thus, measuring the nuclide concentration in both surface and subsurface samples, in theory, allows one to estimate both the exposure age and the erosion rate. This application, again, requires accurate estimates of subsurface production rates due to muons, and, in general, the accuracy of the exposure age estimate scales directly with the accuracy of the subsurface production rate estimate. That is, a 20% uncertainty in the subsurface production rate estimate will directly scale into a 20% uncertainty in the derived exposure age.

The common feature of burial-dating and depth-profile dating applications is that, in most cases, samples collected in the subsurface have been at close to the same depth since they were emplaced. Thus, these applications require accurate estimates of the production rate due to muons at specific depths, which, in turn, requires one of the methods based on downward propagation of the surface muon spectrum, that is, Method 1A or Method 1B. As expected from physical principles and as shown by the fact that a simple exponential approximation for the production rate due to muons cannot be fit to calibration data from sites that span a range of erosion rates, a single global exponential approximation is not adequate for predicting production rates at arbitrary location and depth.

However, it is also important to note that in most burial-dating and depth-profile dating applications, it is only necessary to compute subsurface production rates for a relatively small depth range at a particular site. For example, if one collects samples between 500 and 1000 g cm^{-2} depth in a landform that is 100,000 years old and eroding at no more than 4×10^{-4} g cm^{-2} yr^{-1} (that is, 2 m Myr^{-1} for alluvial sediment with density 2 g cm^{-3}), it is only necessary to estimate production rates in the range 500-1040 g cm^{-2}. Given a restricted depth range as in this example, one can construct a site-specific exponential approximation to subsurface production rates computed using Model 1A or 1B, and use that approximation to simplify further calculations without significant loss of accuracy. Figure 14 shows an example that uses a sum of two exponential functions; other examples include Granger and Smith (2000) and Balco et al. (2011a), who used sums of three exponential functions to approximate muon production rates at specific sites. A similar approach is described by Stone et al. (1998), who used polynomial functions in $\log(z)$ for this purpose. To summarize, the important point here is that in burial-dating and depth-profile applications when one only needs information about muon production rates in a relatively small depth range, one can use a site-specific exponential approximation withouth loss of accuracy. However, an exponential approximation accurate at one site will not be accurate for any other location, except by accident.

Finally, I attempt to estimate the total uncertainty in estimating the nuclide production rate due to muons at a arbitrary location and depth using Model 1A or 1B (or a site-specific approximation thereto). Obviously, this estimate is necessary for computing the contribution of uncertainty in muon production rate estimates to the total uncertainty in a burial or depth-profile age. How to estimate this uncertainty, however, is not at all obvious. Simply attempting to compute an overall misfit or scatter between measurements and predictions for all the calibration sites would likely be incorrect because of the ambiguity in whether agreement or disagreement between model calculations reflects accuracy or inaccuracy in the steady-erosion assumption, or the production model. In many cases one could compensate for a failure of the scaling model by adjusting the erosion rate to obtain a good fit between predictions and measurements regardless.

One can potentially obtain an upper limit on the global uncertainty in predicting muon production rates for arbitrary depth and location by comparing model predictions calibrated at Beacon Heights to observations at Cuiaba, which is the site besides

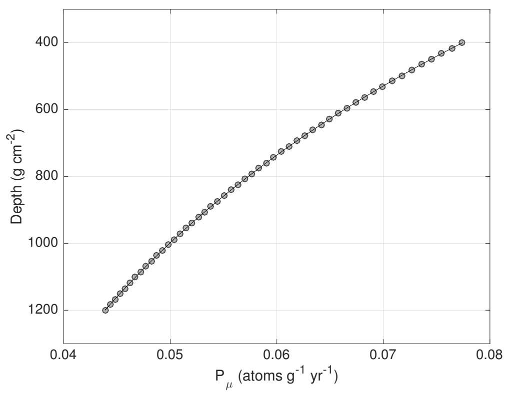

Figure 14: Example of a site-specific exponential approximation to muon production rates computed using Model 1A over a limited depth range. Circles are ^{10}Be production rates computed using Model 1A for depths between 400 and 1200 g cm^{-2} at 1000 m elevation; black line is a best-fitting sum of two exponentials (specifically, $P_{mu} = 0.0413\exp(-z/3264) + 0.0669\exp(-z/811)$). Scatter of the Model 1A production rate estimates around the approximation is less than 0.1%.

Beacon Heights at which the steady-erosion assumption is least important (and in addition it is the site that has the largest scaling difference from Beacon Heights). The data from Cuiaba show scatter well in excess of measurement uncertainty in relation to any model prediction that is smooth in depth – the scatter around any exponential or linear fit to the data from the deep site is at least 30%, compared to mean measurement uncertainty near 15% – so it is hard to evaluate any model fit purely on the basis of this scatter metric. A potentially more useful strategy would be to try to put an upper bound on the total scaling uncertainty for the muon production rate models by assuming that the erosion rate at Cuiaba is 0.8 m Myr^{-1}, as inferred from the spallogenic nuclide inventory at the surface. If we use Model 1A to compute subsurface nuclide concentrations on this basis, we find that predicted ^{10}Be concentrations underestimate measured concentrations at depths >1000 g cm^{-2} by 25% (± 28%). Of course, a 25% difference is not significant at high confidence given 28% scatter, and in addition this estimate depends on the amount of soil cover assumed for the lower site at Cuiaba. If we reduce the assumed soil thickness to 900 g cm^{-2}, which is likely permitted based on the published description of the site, there would be zero systematic offset between the measurements and the Model 1A predictions (Model 1B would still underestimate measurements by 30%), but on the other hand this would reduce agreement between ^{10}Be concentrations at the deep and shallow sites. Overall, however, I argue from this reasoning that 25% is an upper bound for the total uncertainty in predicting ^{10}Be and ^{26}Al production rates due to muons at arbitrary location and depth using Model 1A (the corresponding figure for Model 1B is 50%). In other words, the 25% difference between predictions and observations at this site as calculated above is due to (i) inaccuracy in estimating the soil cover thickness; (ii) possible unsteady erosion; (iii) measurement uncertainty; and (iv) inaccuracy in the muon production rate scaling. Thus, an upper bound on the uncertainty in (iv), the muon production rate scaling, must be less than 25% (for Model 1A) or 50% (for Model 1B). It is, in addition, certainly possible – and it is impossible to disprove – that total scaling uncertainty for muon production using Model 1A is no larger than scaling uncertainty for spallogenic production, which has been estimated from scatter in surface production rate calibration data to be in the range of 6-10% (Borchers et al., 2016).

To summarize, I propose that the total uncertainty in computing subsurface muon production rates at arbitrary location and depth using Model 1A is less than 25% under any circumstances and, by analogy with better estimates for scaling accuracy for spallogenic production, likely 10% or better in most cases (i.e., where the scaling difference between Beacon Heights and the site of interest is much smaller than that between Beacon Heighs and Cuiaba). On the other hand, available evidence indicates the uncertainty in computing production rates using Model 1B may be larger, possibly as much as 50%. Calibration data are not sufficient to make a more precise estimate of the global scaling uncertainty for these production models; the most efficient way to address this problem would most likely be to collect additional calibration data from a bedrock core at a low-elevation, low-erosion-rate site similar to Cuiaba.

9. Needed accuracy/precision for surface exposure dating applications.

Surface exposure dating is a much less demanding application of muon production rate calculations for two reasons. First, muon production is a small fraction of total surface production. Second, samples that can be accurately exposure-dated are by definition at sites where the surface erosion rate is very low, so it is not necessary to have any information about the production rate below a few centimeters depth. Assume, for example, that surface production due to muons is 2% of total surface production. If we accept the argument above that muon production rates calculated using Model 1A calibrated at Beacon Heights are accurate to better than 25% in all cases, this implies that the uncertainty in estimating the total surface production rate at an arbitrary location that is attributable to scaling uncertainty in Model 1A is only 0.5%. This is substantially less than the uncertainty in scaling spallogenic surface production, which is generally believed to be at least ~6% (Borchers et al., 2016). Note that this is not necessarily true for exposure-dating using in-situ-produced ^{14}C in quartz: production of ^{14}C by muons accounts for up to 20% of total surface production. Thus, for ^{14}C, a 25% uncertainty in estimating muon production rates would equate to a 5% uncertainty in the total surface production rate estimate. On the other hand, this indicates that surface production rate calibration data for ^{14}C can potentially provide some constraints on the uncertainty in scaling muon production rates. However, I have not pursued that approach further here.

To summarize, Model 1A appears to have substantially better than needed accuracy for exposure-dating applications using ^{10}Be and ^{26}Al. Of course, Model 1A is also computationally quite complicated. If it is also more precise than necessary, this suggests that a much simpler approximation of surface production rates due to muons would be adequate for ^{10}Be and ^{26}Al exposure dating. Surface production rates predicted by Model 1A can be accurately approximated by:

$$P_{\mu,i,0}(h) = P_{\mu,SL,i} \exp\left[\frac{(1013.25 - h)}{L_i}\right] \quad (7)$$

Here $P_{\mu,i,0}(h)$ is the total (including both negative muon capture and fast muon interactions) surface production rate of nuclide i due to muons (atoms g^{-1} yr^{-1}) at atmospheric pressure h (hPa), $P_{\mu,SL,i}$ is a nominal surface production rate (atoms g^{-1} yr^{-1}) of nuclide i due to muons at sea level (1013.25 hPa), and L_i is an effective e-folding length in atmospheric pressure for nuclide i (hPa). Note that although atmospheric attenuation of the muon flux is independent of the nuclide being produced, it is dependent on muon energy. Because the proportion of production due to negative muon capture and fast muon interactions varies by nuclide, production of each nuclide involves a different part of the muon energy spectrum, and the value of L_i in this formula is specific to each nuclide. As shown in Figure 15, Equation 7 can be fit to surface production rates predicted by Model 1A quite accurately; the maximum difference between the Model 1A predictions and the approximation with best-fitting parameters in the range 450-1013.25 hPa is 2% (^{10}Be) and 1% (^{26}Al). The best fitting parameters are $P_{\mu,SL,10} = 0.0735$ atoms g^{-1} yr^{-1}, $P_{\mu,SL,26} = 0.6764$ atoms g^{-1} yr^{-1} $P_{\mu,SL,14} = 3.067$ atoms g^{-1} yr^{-1}, $L_{10} = 299.2$ hPa, $L_{26} = 288.0$ hPa, and $L_{14} = 267.8$ hPa. This is very similar to the elevation scaling formulae proposed by Braucher et al. (2013) and Lal (1991), and highlights the fact that although simple exponential approximations for muon production rate scaling are not globally accurate for arbitrary location and depth, they are more than accurate enough for some geological applications.

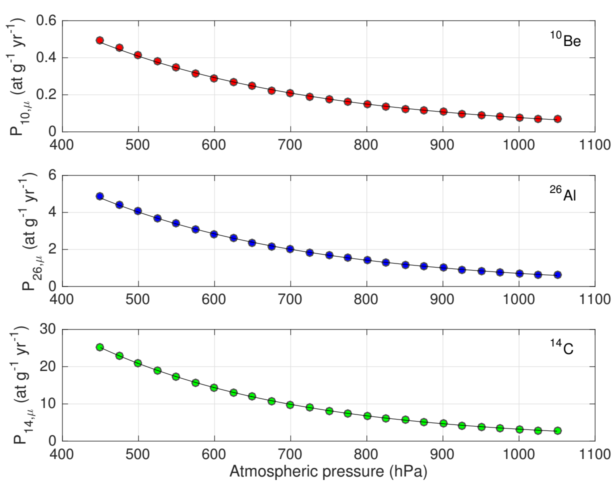

Figure 15: Circles are total surface production rates due to muons predicted by Model 1A (with $\alpha = 1$) as calibrated at Beacon Heights for ^{10}Be (top), ^{26}Al (middle), and ^{14}C (bottom). Lines show Equation 7 fit to the Model 1A predictions.

To summarize, Model 1A has better accuracy than needed in estimating surface production rates due to muons for exposure-dating applications using ^{26}Al and ^{10}Be, and surface production rates computed by Model 1A can be fit very precisely by a single exponential function in atmospheric pressure. Thus, the simple approximation in Equation 7 is accurate enough for exposure-dating applications. If this had been recognized by Balco et al. (2008), they could have saved a lot of computation time in exposure-dating calculations.

Note that for exposure-dating applications it is also necessary to have some information about the depth-dependence of production due to muons, because computing the exposure age of sites with non-negligible surface erosion rates requires integrating production rates with respect to depth. For typical exposure-dating applications at sites with exposure ages of tens of thousands of years, surface erosion rates are in the range of millimeters per thousand years or lower. Thus, for most exposure-dating applications, samples have not been more than ~10 cm below the surface during the period of exposure. This implies that for exposure-dating applications we only need an estimate of the effective e-folding length of production due to muons in the upper few centimeters below a rock surface. Figure 16 shows an estimate of this quantity derived by using Model 1A to compute production rates due to muons at 0 and 10 g cm^{-2} and deriving an effective e-folding length from these values. Note that this calculation is not possible using Model 1B because of a numerical artifact in the code of Lifton et al. (2014) that causes calculated production rates due to negative muon capture to spuriously increase with depth between 0-10 g cm^{-2} depth at some locations.

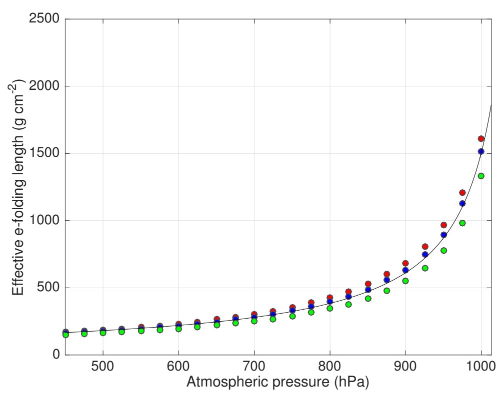

Figure 16: Circles are effective e-folding lengths in upper 10 g cm^{-2} for production of ^{10}Be (red), ^{26}Al (blue), and ^{14}C (green) by muons, calculated using Model 1A with α = 1, calibrated to the Beacon Heights data. The solid line is the approximation given by Equation 8.

The effective e-folding length for production due to muons immediately below the surface is quite variable with elevation. This was not recognized by Balco et al. (2008), who used a single representative value without regard for elevation. As shown in Figure 16, it can be approximated by the following relationship:

$$\Lambda_{\mu,eff} = (a + bh)^{-1} \quad (8)$$

Where $\Lambda_{\mu,eff}$ is the effective e-folding length (g cm^{-2}) for muon production in the uppermost 10 g cm^{-2} below the surface, h is atmospheric pressure (hPa), a = 0.01036, and $b = -9.697 \times 10^{-6}$.

To summarize this section up to this point, if we accept that Model 1A is accurate enough for typical exposure-dating applications, the approximation to Model 1A given by Equations 7 and 8 is also accurate enough for these applications. Thus, for most surface exposure dating calculations, it is not necessary to expend computation time on fully evaluating the Model 1A code. These approximations are good enough.

I now address the issue of the differences between Models 1A and 1B in scaling surface production rates due to muons, as they relate to surface exposure-dating applications. Model 1A assumes that the muon flux varies with atmospheric pressure, but not with geomagnetic cutoff rigidity. Model 1B assumes that the muon flux varies with both atmospheric pressure and cutoff rigidity. It also allows for variation in the muon flux with solar modulation, but this is of relatively minor importance; in applying Model 1B throughout this paper I assume that the solar modulation constant is the mean Holocene value according to Lifton et al. (2014).

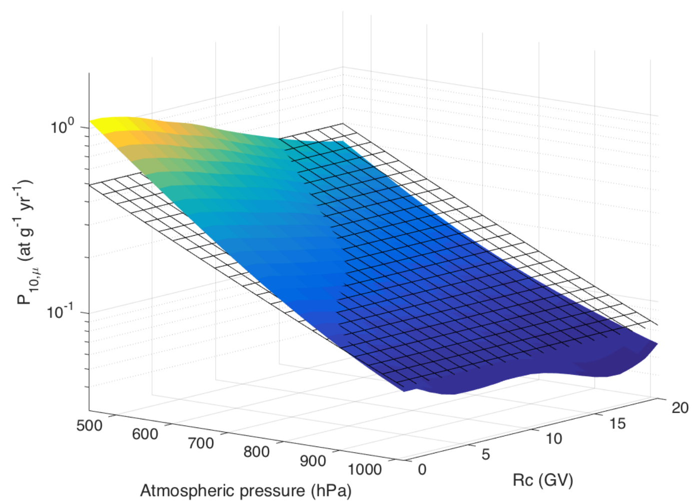

Figure 17: Surface production rate of ^{10}Be due to muons predicted by Models 1A and 1B. Model 1A (transparent mesh) is variable only with atmospheric pressure. Model 1B (colored surface) varies with both atmospheric pressure and geomagnetic cutoff rigidity.

Figure 17 shows the difference between these scaling models, both with cross-sections calibrated at Beacon Heights. Differences in predicted surface production rates due to muons are as large as 50% in some parts of the space represented in the figure. This figure also highlights an apparent numerical artifact in the Model 1B scaling method: the periodic variation in production rate with cutoff rigidity that is evident near sea level pressure in this figure is not expected from the physics of muon production. This effect originates in calculations of negative muon capture production in the Model 1B code and is possibly a spurious result of differencing polynomial approximations for muon energy spectra used by Sato et al. (2008) and thence by Lifton et al. (2014). This apparent artifact, as well as the observation described above that Model 1B appears to over-scale production rates between Beacon Heights and Cuiaba, both indicate inaccuracies in Model 1B. However, it is also clear from basic physical principles that production rates due to muons should, in fact, vary with cutoff rigidity, so even though Model 1A appears to perform well to the extent that it can be tested against calibration data, it is likely oversimplified. Thus, I now ask how large an inaccuracy could be introduced into surface exposure-dating calculations if, in fact, model 1B is correct and Model 1A is not.

Figure 18 shows the results of this calculation. For ^{26}Al and ^{10}Be, not knowing whether Model 1A or Model 1B is correct has a negligible (e.g., less than 1%) effect on the total surface production rate estimate for nearly all locations. At very high cutoff rigidities (> 15 GV), which are predicted to occur rarely and infrequently by most paleomagnetic reconstructions so are largely irrelevant for nearly all practical purposes, differences approach 2%. Figure 18 also shows that existing ^{10}Be and ^{26}Al production rate calibration data (surface production rate calibration data relevant to calibrating spallogenic production rates, not subsurface data relevant to calibrating muon production models as discussed in this paper) are subject to minimal uncertainty (< 0.5% in all cases) from this effect. Thus, not knowing which muon scaling model is preferable will not introduce any systematic bias into calibration of spallogenic production rates for ^{26}Al and ^{10}Be using available data. However, a percent-level error might be introduced if subsequently using this calibration to compute exposure ages at low elevation and low latitude.

For ^{14}C, on the other hand, not knowing whether Model 1A or 1B is correct introduces significant (i.e., > 5%) uncertainty in total production rate estimates at low-elevation sites. As I briefly discuss above but do not pursue further in this paper, existing ^{14}C production rate calibration data from surface samples (Figure 18) could potentially provide some constraints on which model is correct.

It would be possible to further limit the effect of not knowing whether Model 1A or 1B are correct on surface exposure dating applications by using a smoothed approximation intermediate between the two models, that shows less variability with Rc than Model 1B but more than 1A, and also smooths out apparent polynomial artifacts in Model 1B. An example approximation with these properties for ^{10}Be would be:

$$P_{\mu,10,0}(h, R_C) = \left(0.07 - \frac{0.015R_C}{20}\right)\exp\left[\frac{(1013.25 - h)}{250 + 2.5R_C}\right] \quad (9)$$

The maximum difference in the total surface ^{10}Be production rate estimate between this approximation and the predictions of either Model 1A or 1B is less than 0.2% for available calibration sites and does not exceed 0.6% for atmospheric pressure between 450-1013.25 hPa and R_C between 0-15 GV. Overall, I conclude that either the approximation to Model 1A given in Equations 7 and 8, or a smoothed intermediate model such as that given by Equation 9 with subsurface attenuation lengths estimated from Equation 8, will yield acceptable accuracy for surface exposure dating applications us-

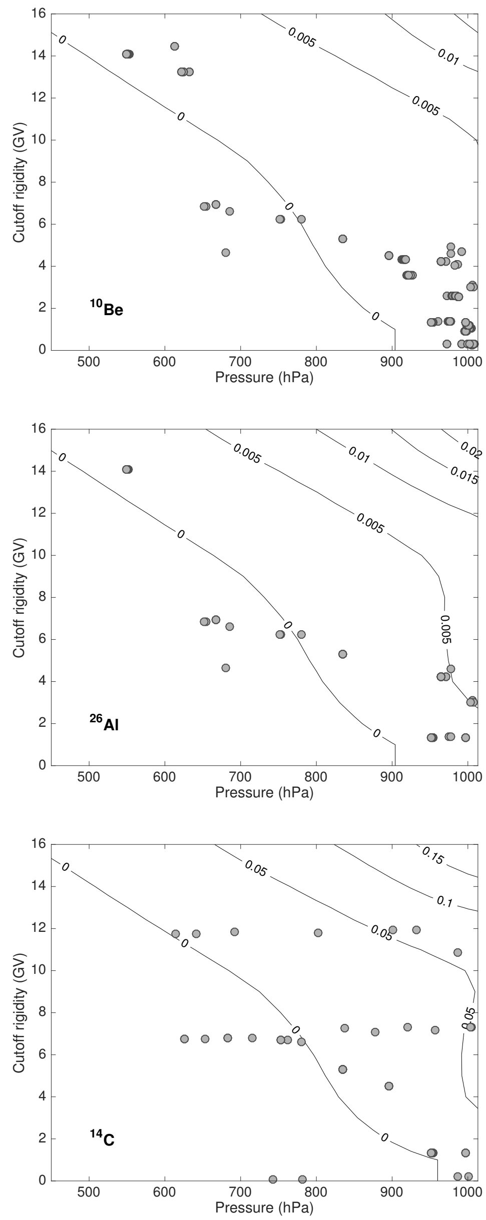

Figure 18: Effect on total surface ^{10}Be (top), ^{26}Al (middle), and ^{14}C (bottom) production rate estimates (including both spallation and muons) of not knowing whether Model 1A or 1B is correct. The contoured field is the difference in predicted production rates due to muons between models as a fraction of the total surface production rate (e.g., the contour labeled '0.01' indicates that the difference between models is 1% of the total production rate). Circles are locations of ^{10}Be and ^{26}Al calibration data from the ICE-D production rate calibration database (calibration.ice-d.org) and ^{14}C calibration data from Borchers et al. (2016).

ing ^{26}Al and ^{10}Be while minimizing computation time. Basically, if muons account for 2% of surface production, one should not have to devote 98% of computation time to them in surface exposure dating applications. This analysis shows that in nearly all practical applications of exposure-dating, a highly simplified approximation is adequate. Although this conclusion also holds for ^{14}C measurements at most locations, it may not for some measurements at low elevation and low latitude.

10. Needed accuracy/precision for erosion rate estimates.

Estimating erosion rates for either single locations or entire catchments involves solving Equation 1 at the surface ($z = 0$) for ϵ. If we assume that production is only by fast neutron spallation and take $N_{0,i}$ to be the surface concentration and $P_{0,i}$ the surface production rate of nuclide i, this reduces to:

$$N_{i,0} = \frac{P_i}{\lambda_i + \frac{\epsilon}{\Lambda_{sp}}} \tag{10}$$

This is explicit in ϵ so can be directly solved to yield:

$$\epsilon = \frac{\Lambda_{sp}}{N_{0,i}} \left(P_i - N_{0,i}\lambda_i \right) \tag{11}$$

This formula has been commonly used to relate nuclide concentrations in rock surfaces or stream sediment to erosion rates (e.g., Lal, 1991). If we include production by muons as well as spallation, we have:

$$N_{0,i} = \frac{P_{sp,i}}{\lambda_i + \frac{\epsilon}{\Lambda_{sp}}} + \int_0^{\infty} P_{\mu,i}(\epsilon t) e^{-\lambda_i t} dt \tag{12}$$

Even if we approximate the depth dependence of production rates due to muons by an exponential function, this is still implicit in ϵ, so requires an implicit solution method. If one wants to use Model 1A or 1B to compute the right-hand term, repeated numerical integrations are necessary to evaluate the integral in the second term in the equation, and in addition the integral will need to be evaluated multiple times during the implicit solution scheme. Thus, if we accept either Model 1A or 1B as the most accurate calculation method for production rates due to muons, then solving Equation 12 for the erosion rate is computationally very time-consuming.

Importantly, however, in computing erosion rates from surface nuclide concentrations by solving Equation 12, it is never necessary to accurately know the production rate due to muons at any particular depth; it is only necessary to know the integrated nuclide concentration in the right-hand term. This suggests that the muon production rate calculation could potentially be highly simplified without loss of accuracy in estimating the erosion rate. Even though an exponential approximation for $P_{\mu,i}(z)$ would still not allow an explicit solution, it would make the implicit solution much faster. To do this, observe that there exists some value for an effective e-folding length $\Lambda_{\mu,eff,i}$ for which the second term in Equation 12 can be represented by a single exponential approximation, that is:

$$\int_0^\infty P_{\mu,i}(\epsilon t)e^{-\lambda_i t}dt = \frac{P_{\mu,0,i}}{\lambda_i + \frac{\epsilon}{\Lambda_{\mu,eff,i}}} \tag{13}$$

Here $P_{\mu,0,i}$ is the surface production rate of nuclide i due to muons, which we can estimate from the simplified approximation to Model 1A given by Equation 7. If we evaluate the integral on the left side of this equation using the Model 1A or 1B code, we can solve the equation for $\Lambda_{\mu,eff,i}$. As described earlier in previous discussion of exponential approximations, $\Lambda_{\mu,eff,i}$ varies with both the atmospheric pressure and the erosion rate, and in the case of Model 1B it also varies with geomagnetic cutoff rigidity.

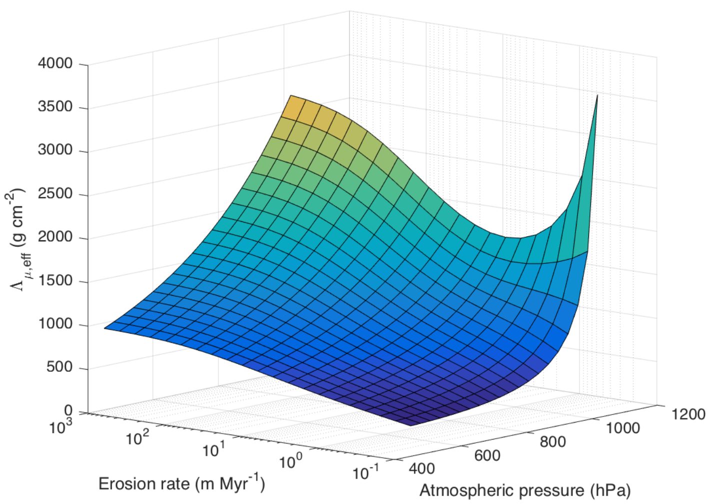

Figure 19: Variation in $\Lambda_{\mu,eff,10}$ with atmospheric pressure and erosion rate, calculated using Model 1A with $\alpha = 1$.

Figure 19 shows the variation in $\Lambda_{\mu,eff,10}$ (that is, appropriate for ^{10}Be) for Model 1A, over the range of atmospheric pressure and erosion rate that is likely to be encountered in practice, on a 20 x 20 grid that is linearly spaced in atmospheric pressure and logarithmically spaced in erosion rate. Having computed $\Lambda_{\mu,eff,10}$ on a grid spanning a range of pressure and erosion rate, one can simplify Equation 12 as follows:

$$N_{0,i} = \frac{P_{sp,i}}{\lambda_i + \frac{\epsilon}{\Lambda_{sp}}} + \frac{P_{\mu,i}}{\lambda_i + \frac{\epsilon}{\Lambda_{\mu,eff,i}(h,\epsilon)}} \tag{14}$$

where the function $\Lambda_{\mu,eff}(h,\epsilon)$ is defined in discrete form by the precalculated grid shown in Figure 19. This is still implicit, but if one uses Equation 7 above to compute $P_{\mu,i}$ at the site, and then evaluates the function $\Lambda_{\mu,eff,i}(h,\epsilon)$ by interpolation from the precalculated grid shown in Figure 19, solving it is computationally trivial. Tests of this procedure against solving Equation 12 by numerical integration using the complete

Model 1A code shows that results of the simplified procedure differ from results calculated using the complete code by less than 0.25% for the entire range of atmospheric pressure and erosion rate shown.

A similar procedure could be developed for Model 1B, except that one would need to determine the dependence of $\Lambda_{\mu,eff,i}(h,\epsilon)$ on geomagnetic cutoff rigidity as well as atmospheric pressure and erosion rate, thus requiring interpolation on a 3-dimensional instead of 2-dimensional grid. To determine if this is necessary, I did an experiment in which I calculated erosion rates at an array of sites spanning a range of atmospheric pressure, cutoff rigidity, and erosion rate using both (i) numerical integration of the full Model 1B code, and (ii) the simplified procedure based on values of $\Lambda_{\mu,eff,i}(h,\epsilon)$ computed using the Model 1A code and shown in Figure 19. In other words, I assumed that Model 1B is correct, but solved Equation 14 using values for $\Lambda_{\mu,eff,i}(h,\epsilon)$ computed using Model 1A. Despite intentionally using internally inconsistent calculation methods in this way, maximum differences in resulting erosion rate estimates were still less than 5% in all cases and less than 1% in 93% of cases. This shows that uncertainty in whether Model 1A or Model 1B is correct contributes negligble uncertainty to erosion rate estimates based on ^{10}Be concentrations.

To summarize, one can use a simple exponential approximation for ^{10}Be or ^{26}Al production by muons for erosion rate calculations without loss of accuracy, as long as the calculation method captures the fact that the effective e-folding length applicable to this calculation varies with location and erosion rate. In the paragraphs above I have proposed a method to do this by computing $\Lambda_{\mu,eff}(h,\epsilon)$ as a function of h and ϵ by interpolation from a coarse grid of precalculated values, which is computationally extremely simple and maintains accuracy at the $< 1\%$ level compared to using the complete Model 1A code. Note that although I have represented this idea by defining an effective e-folding length $\Lambda_{\mu,eff,i}$ that varies with atmospheric pressure and erosion rate, in an actual computational implementation it would be faster and simpler to precompute and store values for the entire second term in Equation 12 on a grid in erosion rate and atmospheric pressure that could be used for interpolation, rather than taking the redundant steps of representing these results as values of $\Lambda_{\mu,eff,i}$ and then using them to recalculate the value of the integral within the implicit solver.

A final note in this section is that in practice the precision of the numerical method of computing an erosion rate from a surface nuclide concentration is not an important limit on the absolute accuracy of the erosion rate estimate. A much more important limit on the accuracy of the erosion rate estimate is that the calculation is based on the assumption that the muon-produced nuclide inventory has reached equilibrium with a steady erosion rate. For relatively long-half-life nuclides like ^{10}Be and ^{26}Al, in nearly all geological situations that can be envisioned, this is unlikely to be the case. Thus, no matter what the precision of the numerical solution method, whether or not the erosion rate estimate accurately represents the true erosion rate is much more sensitive to the geological assumptions necessary to do the calculation at all.

11. Conclusions

Models for production of ^{26}Al, ^{10}Be, and ^{14}C in quartz by cosmic-ray muons that are based on downward propagation of the surface muon energy spectrum using the method described by Heisinger can, in general, successfully match existing subsurface calibration data. However, using these calibration data as a quantitative test for the accuracy of methods for geographic scaling of the surface muon flux is not conclusive, because erosion rates at most available calibration sites are too high to effectively decouple production rate estimates from the steady-state erosion assumption.

A possible exception is that a comparison between the two lowest-erosion-rate sites at Beacon Heights (high elevation, high latitude) and Cuiaba (low elevation, low latitude) shows that the implementation of Heisinger's method in Balco et al. (2008) (referred to here as Model 1A), appears to perform better than the similar implementation in Lifton et al. (2014) that uses more complex geographic scaling (here, Model 1B). Physical arguments indicate that geographic scaling in Model 1B, which includes variation in the muon flux with magnetic cutoff rigidity, should be more accurate for geographic scaling of muon flux than Model 1A, which does not include such variation. However, Model 1B overestimates the difference in production rates between Beacon Heights and Cuiaba. In addition, the Model 1B code of Lifton et al. (2014) predicts some physically unexpected and likely spurious production rate variations that may originate from approximations used in the code. Thus, despite the expectation that Model 1B should perform better than Model 1A, available data indicate that it does not. This conclusion, however, is weak and could be better evaluated by generating new calibration data from sites with erosion rates on the order 0.1 m Myr^{-1} or less, at lower elevation and lower latitude than Beacon Heights. Preferably these data would be from a borehole in a bedrock surface where sample depths are accurately known and not subject to the uncertainties that arise from opportunistic sampling at mine excavations.

Burial-dating and depth-profile dating applications require precise estimates of production rates due to muons at specific depths, so in nearly all cases for these applications it is necessary to use one of the models based on downward propagation of the muon energy spectrum, that is, either Model 1A or 1B. An upper limit on the absolute uncertainty in subsurface production rates for ^{26}Al and ^{10}Be computed using Model 1A, to the extent it can be determined from available calibration data, is 25% globally, but it is likely that actual uncertainties are closer to 10%, similar to scaling uncertainties for spallogenic production. For burial-dating and depth-profile applications, simplified exponential approximations to subsurface production rates can be fit to a limited depth range at a specific site in order to speed up production rate calculations relative to the complete Model 1A or 1B codes. However, global scaling models based on a simple exponential approximation to calibration data are oversimplified for this purpose.

For surface exposure dating applications using ^{10}Be and ^{26}Al in quartz, the muon-produced nuclide inventory is typically a small fraction of the total measured nuclide concentration in surface samples. Thus, a highly simplified scaling method that represents the surface production rate due to muons by a simple exponential function of atmospheric pressure can be used without significant loss of accuracy in relation to more complex muon scaling models. With some exceptions, this is likely also the case for exposure-dating with ^{14}C in quartz.

For estimating steady erosion rates from surface ^{10}Be or ^{26}Al concentrations, it is also possible to develop a simple and computationally trivial scaling method, based on an effective attenuation length for muon production that is variable with location and erosion rate, that maintains the numerical precision of the calculation in relation to the computationally time-consuming Heisinger method.

12. Computer code

All calculations in this paper were done using MATLAB (R2015b). Many also require the MATLAB Optimization Toolbox. MATLAB code to perform all calculations and generate all figures is available at the following address:

`http://hess.ess.washington.edu/repository/muons2016/`

13. Acknowledgements.

This work was supported by the Ann and Gordon Getty Foundation. I thank Régis Braucher and Martin Lupker for helpful and comprehensive reviews.

Arnold, M., Merchel, S., Bourlès, D. L., Braucher, R., Benedetti, L., Finkel, R. C., Aumaître, G., Gottdang, A., Klein, M., 2010. The French accelerator mass spectrometry facility ASTER: improved performance and developments. Nuclear Instruments and Methods in Physics Research Section B: Beam Interactions with Materials and Atoms 268 (11), 1954–1959.

Balco, G., Purvance, M. D., Rood, D. H., 2011a. Exposure dating of precariously balanced rocks. Quaternary Geochronology 6 (3), 295–303.

Balco, G., Rovey, C., 2008. An isochron method for cosmogenic-nuclide dating of buried soils. American Journal of Science 308, 1083–1114.

Balco, G., Shuster, D., Blard, P., Zimmermann, L., Stone, J., 2011b. Cosmogenic 21ne production systematics in quartz inferred from a 25-meter sandstone core. Mineral. Mag 75, 473.

Balco, G., Stone, J., Lifton, N., Dunai, T., 2008. A complete and easily accessible means of calculating surface exposure ages or erosion rates from ^{10}Be and ^{26}Al measurements. Quaternary Geochronology 3, 174–195.

Boezio, M., Carlson, P., Francke, T., Weber, N., Sufffert, M., Hof, M., Menn, W., Simon, M., Stephens, S., Bellotti, R., Cafagna, F., Circella, M., DeMarzo, C., Finetti, N., Papini, P., Piccardi, S., Spilllantini, P., Ricci, M., Casolino, M., DePascale, M., Morselli, A., Picozza, P., Sparvoli, R., Barbiellini, G., Schiavon, P., Vacchi, A., Zampa, N., Grimani, C., Mitchell, J., Ormes, J., Streitmatter, R., Bravar, U., Golden, R., Stochaj, S., 2000. Measurement of the flux of atmospheric muons with the CAPRICE94 apparatus. Physical Review D 62 (032007).

Borchers, B., Marrero, S., Balco, G., Caffee, M., Goehring, B., Lifton, N., Nishiizumi, K., Phillips, F., Schaefer, J., Stone, J., 2016. Geological calibration of spallation production rates in the CRONUS-Earth project. Quaternary Geochronology 31, 188–198.

Braucher, R., Bourlès, D., Merchel, S., Romani, J. V., Fernadez-Mosquera, D., Marti, K., Leanni, L., Chauvet, F., Arnold, M., Aumaître, G., et al., 2013. Determination of muon attenuation lengths in depth profiles from in situ produced cosmogenic nuclides. Nuclear Instruments and Methods in Physics Research Section B: Beam Interactions with Materials and Atoms 294, 484–490.

Braucher, R., Brown, E., Bourlès, D., Colin, F., 2003. In situ produced ^{10}Be measurements at great depths: implications for production rates by fast muons. Earth and Planetary Science Letters 211 (3), 251–258.

Braucher, R., Merchel, S., Borgomano, J., Bourlès, D., 2011. Production of cosmogenic radionuclides at great depth: A multi element approach. Earth and Planetary Science Letters 309 (1), 1–9.

Dunai, T., 2010. Cosmogenic Nuclides: Principles, Concepts, and Applications in the Earth Surface Sciences. Cambridge University Press: Cambridge, UK.

Fink, D., Smith, A., 2007. An inter-comparison of ^{10}Be and ^{26}Al AMS reference standards and the 10 be half-life. Nuclear Instruments and Methods in Physics Research Section B: Beam Interactions with Materials and Atoms 259 (1), 600–609.

Granger, D., 2006. A review of burial dating methods using ^{26}Al and ^{10}Be. In: Siame, L., Bourlès, D., Brown, E. (Eds.), In-situ-produced cosmogenic nuclides and quantification of geological processes: Geological Society of America Special Paper 415. Geological Society of America, pp. 1–16.

Granger, D. E., Smith, A. L., 2000. Dating buried sediments using radioactive decay and muogenic production of ^{26}Al and ^{10}Be. Nuclear Instruments and Methods in Physics Research Section B: Beam Interactions with Materials and Atoms 172 (1), 822–826.

Heisinger, B., Lal, D., Jull, A. J. T., Kubik, P., Ivy-Ochs, S., Knie, K., Nolte, E., 2002a. Production of selected cosmogenic radionuclides by muons: 2. Capture of negative muons. Earth and Planetary Science Letters 200 (3-4), 357–369.

Heisinger, B., Lal, D., Jull, A. J. T., Kubik, P., Ivy-Ochs, S., Neumaier, S., Knie, K., Lazarev, V., Nolte, E., 2002b. Production of selected cosmogenic radionuclides by muons 1. Fast muons. Earth and Planetary Science Letters 200 (3-4), 345–355.

Hidy, A. J., Gosse, J. C., Pederson, J. L., Mattern, J. P., Finkel, R. C., 2010. A geologically constrained Monte Carlo approach to modeling exposure ages from profiles of cosmogenic nuclides: An example from Lees Ferry, Arizona. Geochemistry, Geophysics, Geosystems 11 (9).

Jull, A. T., Scott, E. M., Bierman, P., 2013. The CRONUS-Earth inter-comparison for cosmogenic isotope analysis. Quaternary Geochronology.

Kim, K., Englert, P., 2004. Profiles of in situ ^{10}Be and ^{26}Al at great depths at the Macraes Flat, East Otago, New Zealand. Earth and Planetary Science Letters 223 (1), 113–126.

Kim, K., Lal, D., Englert, P., Southon, J., 2007. In situ ^{14}C depth profile of subsurface vein quartz samples from Macraes Flat New Zealand. Nuclear Instruments and Methods in Physics Research Section B: Beam Interactions with Materials and Atoms 259 (1), 632–636.

Lal, D., 1991. Cosmic ray labeling of erosion surfaces: in situ nuclide production rates and erosion models. Earth Planet. Sci. Lett. 104, 424–439.

Lifton, N., Sato, T., Dunai, T. J., 2014. Scaling in situ cosmogenic nuclide production rates using analytical approximations to atmospheric cosmic-ray fluxes. Earth and Planetary Science Letters 386, 149–160.

Lupker, M., Hippe, K., Wacker, L., Kober, F., Maden, C., Braucher, R., Bourles, D., Romani, J. V., Wieler, R., 2015. Depth-dependence of the production rate of in situ ^{14}C in quartz from the leymon high core, spain. Quaternary Geochronology 28, 80–87.

Marrero, S. M., Phillips, F. M., Borchers, B., Lifton, N., Aumer, R., Balco, G., 2016. Cosmogenic nuclide systematics and the CRONUScalc program. Quaternary Geochronology 31, 160–187.

Nishiizumi, K., 2002. ^{10}Be, ^{26}Al, ^{36}Cl, and ^{41}Ca AMS standards: Abstract O16-1. In: 9th Conference on Accelerator Mass Spectrometry. p. 130.

Nishiizumi, K., 2004. Preparation of ^{26}Al AMS standards. Nuclear Instruments and Methods in Physics Research B 223-224, 388–392.

Nishiizumi, K., Imamura, M., Caffee, M. W., Southon, J. R., Finkel, R. C., McAninch, J., 2007. Absolute calibration of ^{10}Be AMS standards. Nuclear Instruments and Methods in Physics Research Section B: Beam Interactions with Materials and Atoms 258 (2), 403–413.

Sato, T., Yasuda, H., Niita, K., Endo, A., Sihver, L., 2008. Development of PARMA: PHITS-based analytical radiation model in the atmosphere. Radiation research 170 (2), 244–259.

Stone, J., Evans, J., Fifield, L., Allan, G., Cresswell, R., 1998. Cosmogenic chlorine-36 production in calcite by muons. Geochimica et Cosmochimica Acta 62 (3), 433–454.

Stone, J. O., 2000. Air pressure and cosmogenic isotope production. Journal of Geophysical Research 105 (B10), 23753–23759.

Tables

Table 1. Best-fitting values of muon production parameters for various production models applied to the Beacon Heights data.

Model	^{10}Be f*	σ_0 (μb)	σ_{190} (μb)	P_0	Λ_μ	Scatter (%) All data	Scatter (%) > 1000 g cm^{-2}	^{26}Al f*	σ_0 (μb)	σ_{190} (μb)	P_0	Λ_μ	Scatter (%) All data	Scatter (%) > 1000 g cm^{-2}
Model 1A (α = 0.75) - see Figure 4	0.00157	0.739	37.8			5.2	5.2	0.0118	10.19	521			10.8	13.3
Model 1A (α = 1) - see Figure 5	0.00191	0.280	53.2			5.0	4.7	0.0133	3.89	739			10.5	12.9
Model 1B (α = 1) - see Figure 6	0.00192	0.237	45.0			5.0	4.8	0.0131	3.26	619			10.5	13.0
Borchers et al. (2015) (similar to Model 1B)	0.00188	0.252	47.9					0.0121	4.03	766				
Laboratory measurements by Heisinger et al.[1]	0.0039 ± 0.0003		94 ± 13					0.022 ± 0.002		1410 ± 170				
Model 2 - see Figure 7				0.084	2501		22.9				0.761	2417		23.7

[1N]ormalized to the 07KNSTD and KNSTD standards for ^{10}Be and ^{26}Al respectively.

1318

Table 2. Results of fitting models 1A (with alpha = 1) and 1B to the La Ciotat and Leymon Quarry bedrock cores.

Core	Latitude	Longitude	Elevation	Atmospheric pressure (hPa)	Rc (GV) (see text)	Production rates due to spallation (atoms/g/yr) (Borchers et al., 2016)		Mean measurement uncertainty > 1000 g/cm2 (%)		Erosion rate estimate from spallogenic inventory		Results of model fitting							
												^{10}Be, Model 1A		^{10}Be, Model 1B		^{26}Al, Model 1A		^{26}Al, Model 1B	
						^{10}Be	^{26}Al	^{10}Be	^{26}Al	E (sp) (^{10}Be) (m/Myr)	E (sp) (^{26}Al) (m/Myr)	E (muons) (m/Myr)	Scatter (%)	E (muons) (m/Myr)	Scatter (%)	E (muons) (m/Myr)	Scatter (%)	E (muons) (m/Myr)	Scatter (%)
La Ciotat	43.179	5.576	310	979.3	4.6	5.04	35.14	10.2	21	21.2 ± 2.2	18.1 ± 2.2	33.4	2.1	28.0	2.4	33.3	27.5	26.8	31.5
Leymon High	42.064	7.013	1246	874.6	5	10.75	74.91	9.4	20.4	17 ± 1.8	17 ± 2	12.1	13.8	11.5	14.8	14.4	18.6	13.7	19.8
Leymon Low	42.065	7.014	1277	871.3	5	11.02	76.72	8.5	18.9	7.7 ± 0.8	13.5 ± 1.6	8.61	9.9	8.0	10.2	10.0	23.5	9.4	24.5

Notes:
Erosion rates are converted to m/Myr assuming a rock density of 2.7 g/cm2
Estimates of atmospheric pressure and magnetic cutoff rigidity (Rc) are described in the text.
Production rate estimates use 'St' scaling scheme and calibration data of Borchers et al. (2016).
Uncertainties on erosion rate estimates from spallogenic inventory include uncertainty in production rate and nuclide concentrations.